A Numerical Model for Safety Vacuum Release System (SVRS)

Final Report Submitted by Dr. Jim C. P. Liou to CPSC, December 23, 2010

(Contract CPSC-S-07-0084)

Table of Contents

A Numerical Model for Safety Vacuum Release System (SVRS)

Final Report Submitted by Dr. Jim C. P. Liou to CPSC, June 28, 2010

(Contract CPSC-S-07-0084)

1. Introduction and Summary

Drain suction entrapment is a potential safety hazard in swimming pools, spas, and hot tubs. Safety vacuum release systems (SVRS) are used to mitigate such hazards. The Consumer Products Safety Commission (CPSC) is studying SVRS to understand better the phenomenon involved so that sound standards can be developed to safeguard consumers. In this effort, CPSC has been conducting experiments and has engaged Dr. Jim Liou to develop a numerical model for SVRS.

This report describes the numerical model and the results. Based on the comparisons between model results and CPSC's physical test data, it is concluded that the model captures the main traits of SVRS, and the model can be used to analyze SVRS behavior under various combinations of modes of vacuum release (pump switch or air vent), steady-state flow rate, suction pipe length, pump horsepower, pump elevation offset, and size of air vent orifice. The effectiveness of using a dual-drain to avoid vacuum conditions is demonstrated through simulations of an example.

The numerical model and its data input module are submitted with this report in electronic form. This model simulates the 11 tests conducted by CPSC. It can also be used to explore "what if" questions pertaining to the CPSC test facility.

2. Main Traits of Vacuum Development and Vacuum Release

Water is recirculated in pools and spas by pumping. The recirculating system consists of a drain sump, a length of piping that conveys water from the sump to pump suction (suction pipe), a centrifugal pump, and a length of piping (discharge pipe) that directs the pumped flow back into the pool. The mass and velocity of the water in the piping represents the inertia of the flow. When the drain sump is blocked, the inertia tends to pull water away from the blocked sump. Because water cannot be pulled away until vaporization takes place, this pulling causes a local pressure reduction and subsequent vaporization at the sump. The pressure at vaporization is around 14 psi below local atmospheric pressure. The vacuum force developed

at a 6-inch diameter sump at 14 psi negative pressure is about 400 lbs, sufficient to cause entrapment.

Vacuum development is just one aspect of the hydraulics of SVRS. As the pressure reduction at the sump is happening, its effect spreads out to the rest of the piping system as pressure and flow waves propagating at a speed on the order of 1000 ft/s. This phenomenon is known as water hammer. As a result of wave propagations and wave reflections from the pool, the water column in the piping slows down and stops. If the pump is tripped (explained below), water will enter the pipe exit from the pool and flow backward toward the sump. Eventually, water will return to the sump, close the vapor cavity, and eliminate the vacuum.

Immediately after the blockage, the decreasing flow causes an increase in the pressure rise across the pump (an inherent characteristic of centrifugal pumps) and a decrease in the pump discharge pressure (demanded by the fixed pool level and the reduced flow). Consequently, the pressure in the suction pipe must decrease. This action may lead to vaporization in the suction pipe, especially near the pump suction where the elevation is often higher. Although the pump discharge pressure is reduced by the reduced flow, the pump head is still higher than the pool level. Water is prevented from entering the discharge pipe from the pool, despite the low pressure in the suction pipe.

When the pump is tripped by a SVRS device, the head that prevents the water from entering the discharge pipe diminishes over time. How fast this head diminishes depends on the pump characteristics and the moment of inertia of the rotating mass (pump, motor and entrained water). When the head is sufficiently diminished, water starts to enter the discharge pipe from the pool. The head differential between the pool and the vapor cavity at the sump accelerates the water column toward the sump. The de-energized pump now impedes the reversed flow as it spins down, reverses, and eventually stops. The characteristics of the pump and moment of inertia of rotating mass influences the timing of vacuum relief. In the case of air vent SRVS, the introduction of air to the pump suction will degrade pump performance and reduce suction. The air vent model will be discussed further.

3. The CPSC's SVRS Test Facility

The development of the test facility was guided by voluntary standards (ASME 2002, ASTM 2004). A schematic of CPSC's test facility is shown in Figure 1. A transparent sump is situated at the bottom of a tank. A suction pipe leads the flow from the sump to a centrifugal pump. The minimum length of the suction pipe is 37 ft. This can be increased to 100 ft. if the pipe

Figure 1 The schematic of CPSC's SVRS test facility (Source: Mark Eilbert of CPSC)

Figure 2 Pump and air vent installation (Source: Mark Eilbert of CPSC)

segment *L* shown in the lower left corner of the schematic is inserted. There are nine elbows and one valve on the suction pipe. This valve is kept wide open. The discharge pipe has a fixed length of 100 ft. There are 16 elbows and three valves on the discharge pipe. These valves are throttled to obtain the desired steady-state flow prior to drain blockage. All pipes are 2-inch rigid schedule 40 PVC pipes. All valves are 2-inch schedule 80 ball valves. The elevation profile of the piping is indicated in the schematic. An interchangeable pump (1/2 or 3 hp) is mounted on a platform with an adjustable height. The platform and the pump are shown in Figure 2.

A mechanical actuator, aligned vertically with the center of the sump, lowers an interrupter element (IE) to the vicinity of the sump, where the flow suction draws the IE toward the opening of the sump and blocks it fully. The IE is a 3.5 inch thick 11 inch diameter foam, made of ethyl vinyl acetate (EVA), with a hardness of 35 Shore 00. The foam blocker has a buoyancy of 11 lbs.

Figure 2 shows the air vent assembly. The controllable air vent is connected to the short horizontal pipe segment that leads to the suction of the pump located near Ps in Figure 1. The vent pipe contains an orifice plate and a spring-retracted air cylinder. Centered in the plate is a sharp-edged orifice with a diameter of 0.14, 0.21, or 0.28 inches. During air vent tests, compressed air is fed to the cylinder which pushes a latex foam pad against the orifice and blocks it. The space containing the compressed air is depressurized by energizing a solenoid valve and opens the space to atmosphere. This action lets the spring retract and jerk the latex foam away from the orifice. Following a time delay, the air vent is triggered open when the pressure in suction pipe is sub-atmospheric, thus allowing air into the suction to release vacuum. Once opened, the air vent remains open, irrespective of the pressure levels in the suction piping.

Seven channels of pressure data are measured. These are:

Designation	Location
Pu	sump
Pvis	suction pipe Venturi inlet
Pvts	suction pipe Venturi throat
Ps	pump suction
Pd	pump discharge
Pvid	discharge pipe Venturi inlet
Pvtd	discharge pipe venture throat

Additional data include the rotational speed of the pump, the position of the top face of the IE, and the trigger time of either the air vent or pump trip device. All data were acquired by a computerized data system with sample frequency of 100 kHz. This data rate is more than sufficient to capture the details of transients in the system.

For each test, the behavior of the IE before and after blocking the sump was filmed using a high-speed camera. The frame rate was either 250 frames per second or 125 frames per second.

4. **Tests Used in Model Development**

The following tests were used in model development.

Table 1: Pump Switch Tests - Parameters and Steady-State Conditions

	Case 1	Case 2	Case 3	Case 4	Case 5
Test date	7/21/09	7/29/09	7/30/09	8/21/09	8/21/09
Test time	13:59:38	14:19:02	14:14:36	10:53:56	11:33:56
Suction pipe length (ft)	100	100	37	37	37
Pump elevation offset (in)	-36	-36	36	-36	-36
Tank depth (in)	34	34	34	34	34
Water temperature (°F)	72	78	77	78	78
Pump horsepower	3	3	3	0.5	0.5
Air vent size (in)	N/A	N/A	N/A	N/A	N/A
Steady-state flow (gpm)	68.4	47	45.4	50.9	51.2
Sump pres. (psia)	16.06	16.06	16.00	16.04	16.08
Pump suction pres. (psia)	8.67	13.21	10.89	13.43	13.46
Pump discharge pres. (psia)	49.38	56.65	54.45	19.91	20.09
Time of blockage (sec)	0.53	0.735	0.921	0.3578	0.4576
Time of pump trip (sec)	1.031	2.297	1.306	0.5590	0.6640
Time of vent opening (sec)	N/A	N/A	N/A	N/A	N/A
Time of release (sec)	3.70	5.20	3.60	2.20	2.20

Table 2: Air Vent Tests - Parameters and Steady-State Conditions

	Case 6-1	Case 6-2	Case 7	Case 8	Case 9-1
Test date	11/9/2009	11/9/2009	11/3/2009	11/3/2009	11/9/2009
Test time	13:29:22	13:36:45	12:07:40	13:43:40	11:59:41
Suction pipe length (ft)	100	100	37	37	37
Pump elevation offset (in)	-36	-36	-36	-36	-36
Tank depth (in)	34	34	34	34	34

Water temperature (°F)	53	53	55	55	51
Pump horsepower	0.5	0.5	0.5	0.5	0.5
Air vent size (in)	0.14	0.14	0.14	0.21	0.21
Steady-state flow (gpm)	47	47	51	50.3	51
Sump pres. (psia)	15.68	15.66	15.69	15.86	15.76
Pump suction pres. (psia)	12.09	12.11	13.12	13.45	13.23
Pump discharge pres. (psia)	19.92	19.47	19.93	19.62	20.07
Time of blockage (sec)	0.01	0.036	0.169	0.075	0.021
Time of pump trip (sec)	N/A	N/A	N/A	N/A	N/A
Time of vent opening (sec)	1.776	1.760	1.594	1.616	1.760
Time of release (sec)	3.403	3.467	no release	2.344	no release

Table 2-continued: Air Vent Tests - Parameters and Steady-State Conditions

	Case 9-2	Case 10-1	Case 10-2	Case 11-1	Case 11-2
Test date	11/9/2009	11/9/2009	11/9//2009	11/9/2009	11/9/2009
Test time	12:13:44	13:52:47	13:59:48	12:54:47	12:53:43
Trial number	2	1	2	1	2
Suction pipe length (ft)	37	37	37	37	37
Pump elevation offset (in)	-36	-36	-36	-36	-36
Tank depth (in)	34	34	34	34	34
Water temperature (°F)	51	54	54	51	51
Pump horsepower	0.5	0.5	0.5	0.5	0.5
Air vent size (in)	0.21	0.14	0.14	0.28	0.28
Steady-state flow (gpm)	46	51	51	51	46
Sump pres. (psia)	15.79	15.67	15.63	15.79	15.60
Pump suction pres. (psia)	13.24	13.05	13.11	13.25	13.23
Pump discharge pres. (psia)	19.82	19.86	19.69	19.95	20.21
Time of blockage (sec)	0.028	0.024	0.035	0.011	0.015
Time of pump trip (sec)	N/A	N/A	N/A	N/A	N/A
Time of vent opening (sec)	1.754	1.770	1.775	1.752	1.776
Time of release (sec)	2.356	no release	no release	2.267	2.277

(Source: Mark Eilbert of CPSC)

The pressures in the table are taken from the data files provided by CPSC. The measured pressures during the steady state prior to drain blockage fluctuated somewhat. The tabulated values represent the steady-state condition for each test. In the early stage (prior to the submittal of the interim report in September 2009) of the model development, these pressures were used in establishing the amount of throttling of the ball valves on the discharge line and in establishing elbow head loss coefficients. In the subsequent development, it was found that some variations in these pressures do not change the simulation results significantly.

Consequently, these pressures were not used. This reduced the data requirement to run the numerical model and enables it to explore "what if" situations where test data are not available. Appendix 1 show the correspondence of the test case designations used in this report and the original data file names used by Mr. Eilbert of CPSC.

5. IE Foam Blocker Behavior

The behavior of the IE is described with the aid of a sequence of 11 photos taken from the Case 2 test by CPSC. See Figure 3. The camera is aimed at the center of the suction pipe inlet. The pressure transducer *Pu* is on the left wall of the sump. The pipe on the right side is blanked off. Images were recorded at 250 frames per second. The time is indicated in the photos. The pressure at the sump and the displacement of the top face of the IE foam are shown in Figure 4.

Figure 3-1

The IE blockage is being lowered to the sump just before blockage.

Figure 3-2

The IE has just blocked the sump inlet. The foam is being sucked into the sump. The sucked-in foam is shaped as a portion of a sphere.

Figure 3-3

The IE foam has stopped deforming. This results in pressure being lowered toward vapor pressure. Vapor cavity appears.

Figure 3-4

The IE foam remains in place while the vapor cavity grows over time. The pressure remains at water's vapor pressure.

Figure 3-5

The vapor cavity volume reaches a maximum.

Figure 3-6

The water column in the piping returns to the sump and splashes on the sump wall. The vapor cavity is being filled by the returning flow.

Figure 3-7

The filling continues. The pressure should remain at the vapor pressure, as long as the vapor cavity exists.

Figure 3-8

The vapor cavity is just about to disappear. There appears to be no significant change in the size and shape of the sucked-in foam as the cavity is being filled.
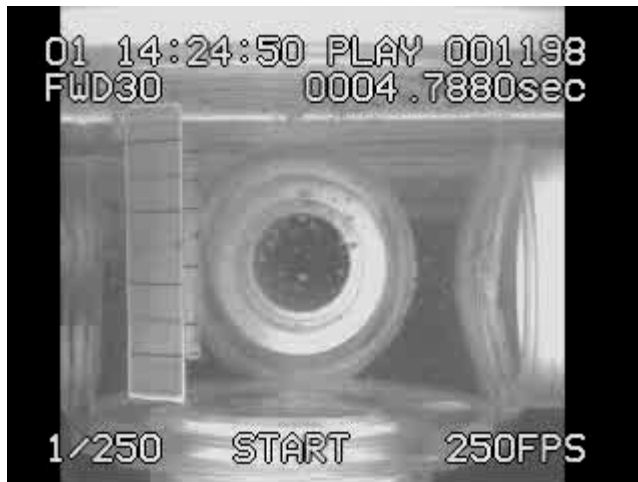
Figure 3-9

The vapor cavity has disappeared and the foam is retracting. The pressure in the sump at this time should be above the vapor pressure. The bubbles visible in the photo are air bubbles.

Figure 3-10

This is the moment just before the foam starts to move up and away as a whole. The foam is still visible at the top of the frame. Notice that the underside of the foam has nearly returned to flat surface. Some air bubbles are visible.

Figure 3-11

The foam has moved away as it is no longer visible at the top of the frame. Some air bubbles are still visible.
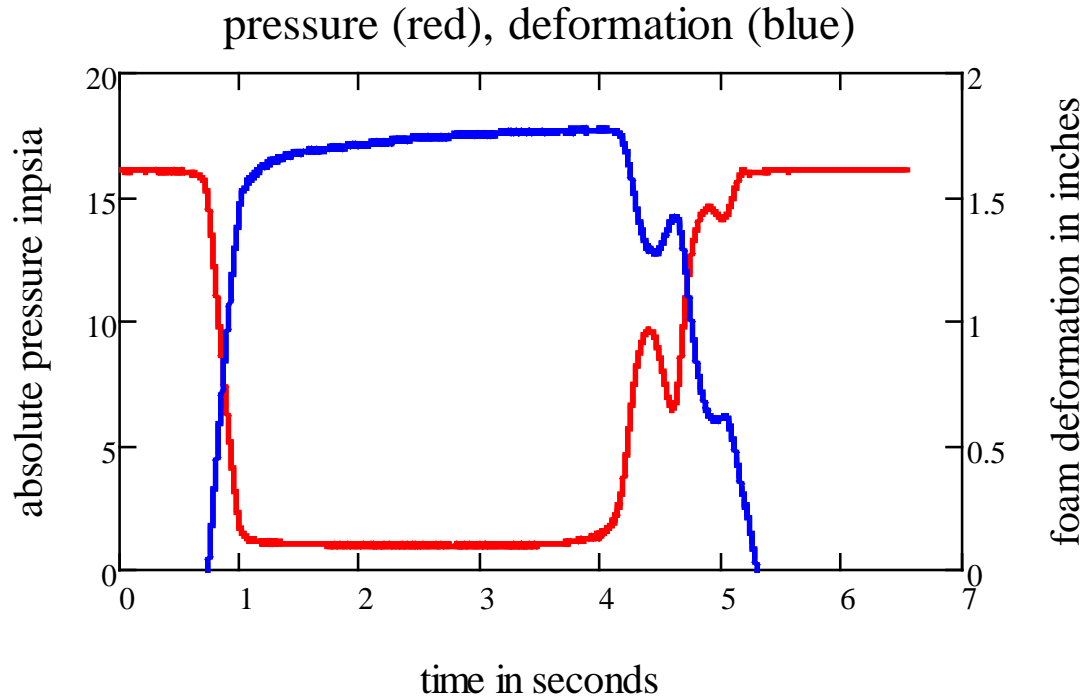
Figure 4 Sump pressure and downward displacement at the top center of the IE foam

Due to instrumentation difficulty, the vertical position of the IE foam was measured at the top center instead of the bottom center of the foam. A dry static test was conducted by CPSC to see if the measured displacement of the top center can be regarded as that of the bottom center. In this test, a vacuum was applied to a blocked sump, where the surrounding air was at atmospheric pressure. The center deformations of the foam, both at the top and at the bottom surfaces, were obtained as a function of vacuum pressure in the sump. The top deformation was measured by a cable transducer, while the bottom was measured by sight and scale. The result is shown in Figure 5. It appears that the bottom deflection follows the top deformation as the whole foam block bends. In other words, there is little relative displacement between the top and the bottom faces of the foam as it is deformed. Therefore, the measured changes in the vertical position of the top face of the IE foam can be taken as the position change of the bottom face.

bottom (blue), top (red)
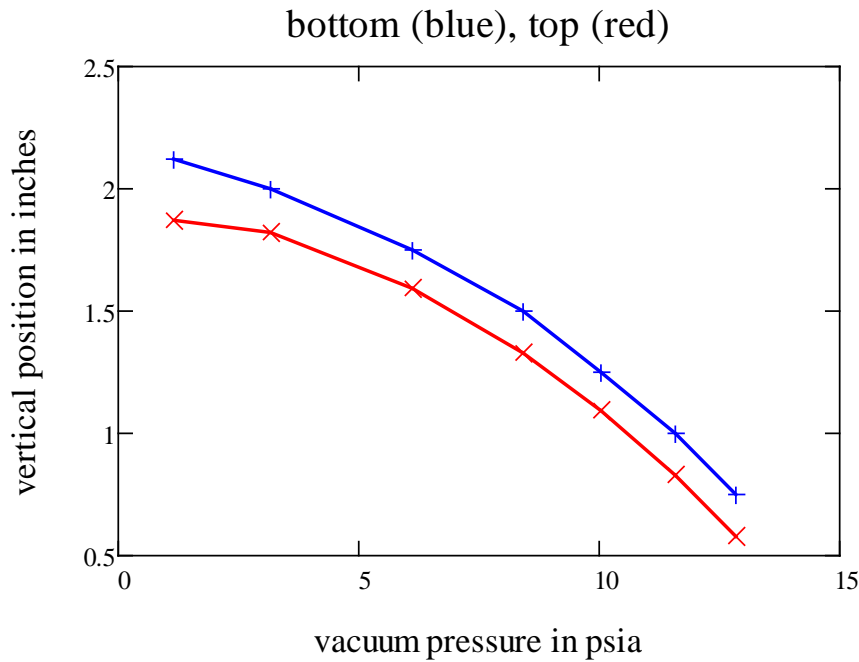
Figure 5 The result of a dry test of foam deformation versus vacuum pressure

The video clip from which Figure 3 was extracted and Figures 3, 4, and 5 reveal that: (1) immediately after the blockage, the center displacement of the IE foam is proportional to the absolute pressure in the sump until the vapor pressure of water was reached; (2) the foam stays deformed when the vapor cavity existed; (3) the foam starts to return to its original shape only after the vapor cavity had disappeared; (4) the underside of the foam returns to a flat surface before the foam moves up and away as a whole; (5) free air (*i.e.*, undissolved air) exists in the system; and (6) the demarcation of vapor cavity formation and collapse is smeared by the free air.

6. Modeling the Foam Blocker

The video reveals that as the flow of water is blocked off suddenly, a portion of the IE foam is being sucked into the sump. This foam deformation provides a temporary volume flux across the sump inlet, which softens the effect of the sudden stoppage of water flow. This softening plays a key role in vacuum development and must be quantified.

Figure 6 shows the IE foam center displacement as a function of sump absolute pressure for Cases 2, 3, 4, and 5 (all five pump switch tests). Figure 7 shows the same for Case 6_1 which is

case 2 (green), 3(magenta), 4(red), 5 (blue)
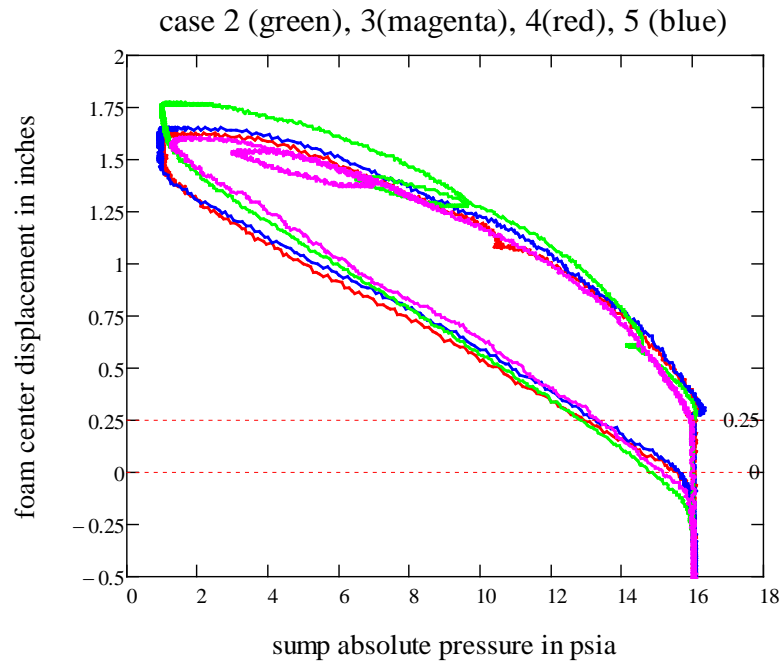
Figure 6 IE foam center vertical displacement as a function of sump absolute pressure for the blocker used in pump switch tests
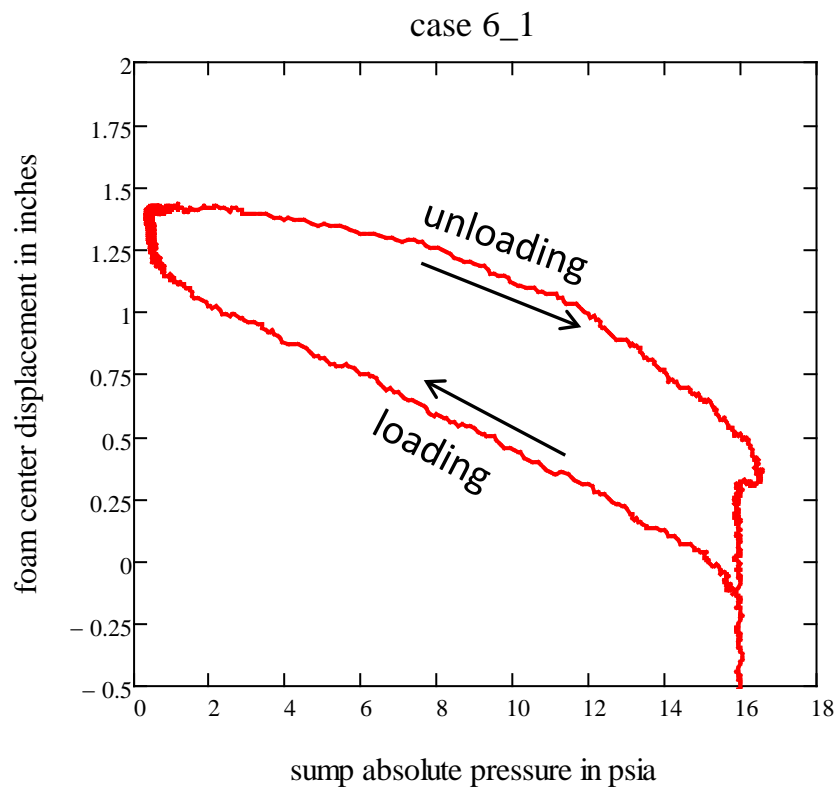
case 6_1

Figure 7 IE   foam center
vertical

displacement as a function of sump absolute pressure for the blocker used in air vent tests representative for all 10 air vent tests. The loci of the foam displacement and sump pressure pair form a loop.

At the steady-state and prior to lowering the IE, the sump is at about 16 psia. There is a slight deformation and sump pressure reduction just before the sump blockage. Once blocked, the center portion of the foam is pulled down by the increasing vacuum in the sump. This phase of the deformation (here called loading phase) tracks the lower limb of the loop. The presence of vapor cavity formation is indicated by the upper left corner of the loop, where a pronounced displacement increase is associated very little decrease in the sump absolute pressure. After the vapor cavity collapse, the foam retracts as the vacuum is being diminished by the return flow. This phase of the deformation (the unloading phase) tracks the upper limb of the loop. Notably, there is still about 0.25 inches of foam displacement when the vacuum is released. This is reasonable as the foam is buoyant and tends to move up before full retraction.

During the unloading phase, the absolute pressure at the sump may temporarily decrease. This causes a "bounce" of the foam while it remains seated. Corresponding to each "bounce" is another but smaller loop in the foam center displacement versus sump pressure plot (see Cases 2 and 3 in the top panel of Figure 6).   Video images of the tests showed that "bounces" are pre-cursers to the foam becoming released. This behavior needs to be modeled.

Comparing Figures 6 and 7, it is seen that for a given amount of sump pressure reduction along the loading limb, the pump switch tests have a greater IE foam displacement increase than that of the air vent tests. The same is also true for the unloading limb.   Thus the IE foam used for the pump switch tests was softer than that used in the air vent tests. Both foam blockers need to be characterized.

The sump blocked with an IE foam is modeled as a capacitance element.   This is depicted in Figure 8. Both the foam and the free air contribute to the capacitance of the sump. There are five unknowns: (1) flow into the suction pipe from the sump Q; (2) volume flux across sump inlet due to foam displacement QB; (3) absolute pressure at the sump P; (4) piezometric head at the inlet of the suction pipe H; and (5) piezometric head at the sump H_s. There are five equations available:

(1) The equation of state of free air:

$$P = \frac{c1s}{V_{old} + dt\,(1-\varphi)(Q_{old} - QB_{old}) + dt\,\varphi\,(Q - QB)}$$ (1)
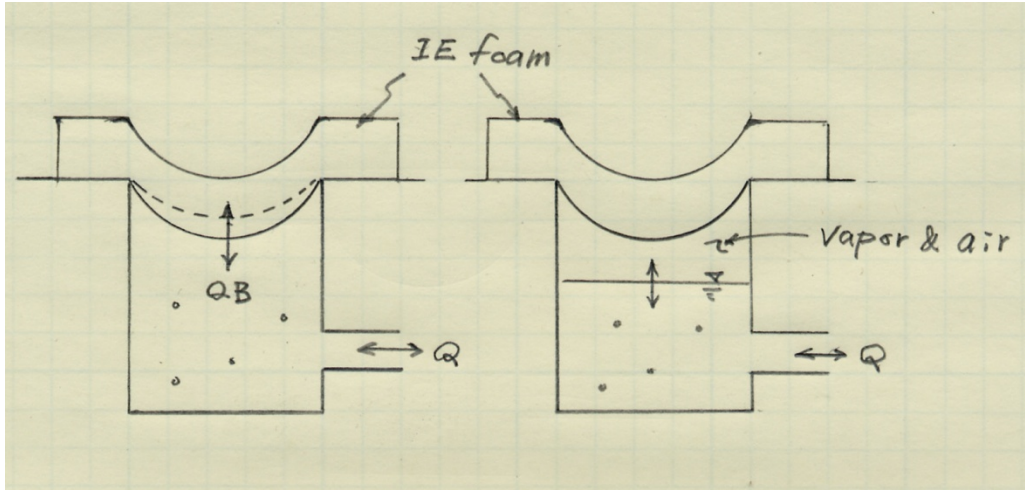
Figure 8 The sump model schematic. The left panel indicates the volume flux QB due to foam displacement. The right panel indicates bulk cavity filled with free air and water vapor. Bubbles of air and vapor in water may present at any time

(2) The pressure - head relationship in the sump:

$$P = \gamma(H_s - \beta_s) \tag{2}$$

(3) The C- compatibility equation for the suction pipe (Wylie and Streeter 1993):

$$H = CM + BM\, Q \tag{3}$$

(4) The volume versus pressure for the sump:

$$[\varphi\, QB + (1 - \varphi)\, QB_{old}]\, dt = \frac{-\gamma\, V_s\, (H_s - H_{sold})}{K} \tag{4}$$

(5) The relationship between the head in the sump and the head at suction pipe inlet:

$$H_s = H + (1 + K_0)\frac{Q^2}{2g\, A^2} \qquad if\ Q > 0 \tag{5}$$

$$H_s = H \qquad if\ Q \le 0 \tag{6}$$

In the above equations, *C1s* = a constant equal to the product of the initial absolute sump pressure, initial void fraction due to the free air, and the initial sump volume, *V* = volume of free air and water vapor mixture, *dt* =time step used in numerical integration, φ = a weighting function in numerical integration (0.75 used throughout), β = sum of sump elevation and the vapor pressure head, *Vs* = sump volume, *A* = pipe cross-sectional area, K_0 = entrance head loss coefficient, and *K* = an equivalent bulk modulus of the blocked sump that varies with sump pressure and have different values for loading and unloading, *CM* and *BM* = suction pipe constants representing pipe impedance and friction (Wylie and Streeter 1993). Subscript *old* denotes quantities at *dt* seconds earlier. Subscript *s* represents quantities at the sump.

The foam displacement versus sump absolute pressure data for Case 2 and Case 6 were used to establish the equivalent bulk modulus (*K*) of a blocked sump. The volume of the foam inside the sump is assumed to be the lower portion of a sphere. Based on the measured foam center displacement, the sump volume, as a function of the measured sump pressure, is represented by Figure 9. The slope of the curves, shown in Figure 10, is the equivalent bulk modulus.

By curve fitting of the measured data, the following quantitative relationships are established:

Pump switch tests

Loading:

$$K = 0.999\,P + 22990 \tag{7}$$

Unloading:

$$K = 164657 - 272.4P + 0.1724P^2 - 3.6485 \times 10^{-5}P^3 \tag{8}$$

Air vent tests

Loading:

$$K = P + 35210 \tag{9}$$

Unloading:

$$K = 110824 - 44.6992P \tag{10}$$

In the above, *K* is in psf and *P* in psfa.

loading (red), unloading (blue)
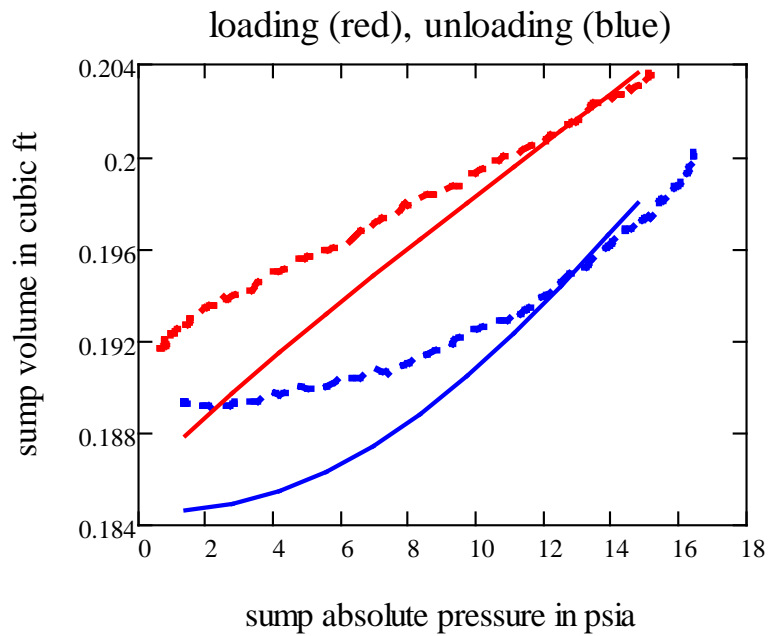
Figure 9 Sump volumes as a function of the absolute sump pressure. Solid lines are for the pump switch   tests. Dotted lines are for   the air vent tests.

loading (red), unloading (blue)
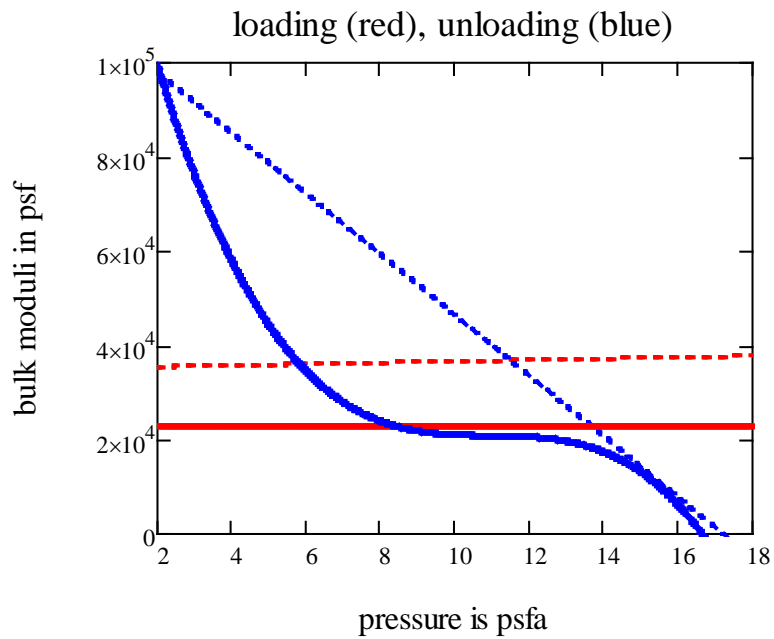
Figure 10 Bulk modulus *K* of the sump during loading and unloading. Solid lines are for the
pump switch tests. Dotted lines are for the air vent tests.

In modeling, the sump absolute pressure over time is monitored. If the pressure is increasing
over a computational time step, the bulk modulus from the unloading limb is used. If the
pressure is decreasing over the time step, the bulk modulus from the loading limb is used. This
algorithm allows the "bounce" described previously to be modeled.

It is believed that the test data have captured relevant aspects of the complex dynamics of the
water surrounding the IE foam on the pool side. The sump appears to be more rigid (*i.e.*, higher
K) in the beginning of the unloading phase because the pool water above the foam has to be
accelerated upward and pushed away as the foam retracts. Once the surrounding water is
mobilized, the retraction becomes easier, and the sump appears to be softer (lower *K*).

The timing of vacuum release is of primary interest. This is handled by keeping track of the
volume of foam inside the sump as a result of volume flux *QB*.

$$S = S_{old} + dt\,[\varphi\,QB + \,(1-\varphi)QB_{old}] \tag{11}$$

S is zero at the very moment when the IE form first contacts the sump. Its value increases or
decreases as demanded by the system dynamics.   The foam blocker is considered released
when *S* becomes zero again.

 7. **Modeling the Centrifugal Pumps**

Modeling the dynamics of the pump and its spinning down after tripping is necessary. The
pumps used in the test are a 3-hp Pentair Challenger high head pump and a ½-hp Sta-Rite spa
pump. The vendor's data are limited to head versus flow curves at 3450 rpm. The rated heads
and flows are not available and have to be estimated. The measured data suggest that the 3-hp
pump was operated near its rated condition prior to tripping, while the ½-hp pump was
operated out on it performance curve (*i.e.*, higher flow and lower head than the rated values).
Furthermore, for the ½-hp pump, the vendor's head versus flow curve gives too high a head for
a specified flow.   Consequently, the vendor's head curve has to be adjusted.

Other estimated data include the rated torque, the four-quadrant pump performance data, and
the moment of inertia of pump and motor. The estimated data for the pumps are shown
below.

Table 3: Estimated Rated Conditions of the Pumps Used in CPSC's Tests

	3-hp pump	½-hp pump
Rated speed (rpm)	3450	3450
Rated head (ft)	80	36
Rated flow (gpm)	98	30
Rated torque (ft-lb)	3.8	0.59
WRR (lb –ft^2)	0.066	0.021
Specific speed (gpm units)	1222	1240

Because both the flow and the pump rotation may reverse, it is necessary to use the pump's head-flow-speed and torque-flow-speed relationships for forward flow-forward rotation (quadrant I), forward flow-reversed rotation (quadrant II), reversed flow-reversed rotation (quadrant III), and reversed flow-forward rotation (quadrant IV). However, only a portion of the head-flow-speed data is available for quadrant I. The rest must be estimated. This is done using the homologous theory (Wylie and Streeter 1993). According to this theory, two pumps with identical specific speed will behave identically. A set of scaled head-flow-speed and torque-flow-speed curves for a centrifugal pump with a specific speed of 1270 (gpm units) is available (Wylie and Streeter 1993) and is shown by solid lines in Figure 11. This set of curves is adopted for this project. The head curve is modified (the dotted line) to reflect the available data. The torque curve is used without any modification because no torque information is available for the two pumps used in the tests.

Upon the drain blockage, the pressure in the sump and in the suction piping is reduced toward the vapor pressure of water. As a result, air bubbles and eventually vapor cavities form. Passage of air bubbles and vapor through the pump will alter the performance of the pump. Through well-instrumented tests, Road et. al., 1983, showed that the voids cause a reduction in the total dynamic head of the pump in quadrant I and an increase in the total dynamic head in quadrant IV. In other words, with voids present, it is more difficult to impart power to the liquid in a forward flow through a forward-rotating pump. And, it is more difficult to push liquid flow backward through a forward-rotating pump. This fact is important to SVRS transients because the pump will be operated in quadrants I and IV.   This study follows the methodology of RELAP5 1992 to establish a pair of degraded head curves that include the maximum effects of free air and vapor on the head performance curve of a centrifugal pump. The degraded head curves are shown in Figure 12. In these figures, v = flow scaled by the rated flow, α = speed scaled by the rated speed, WH and WB represent scaled head and torque curves.
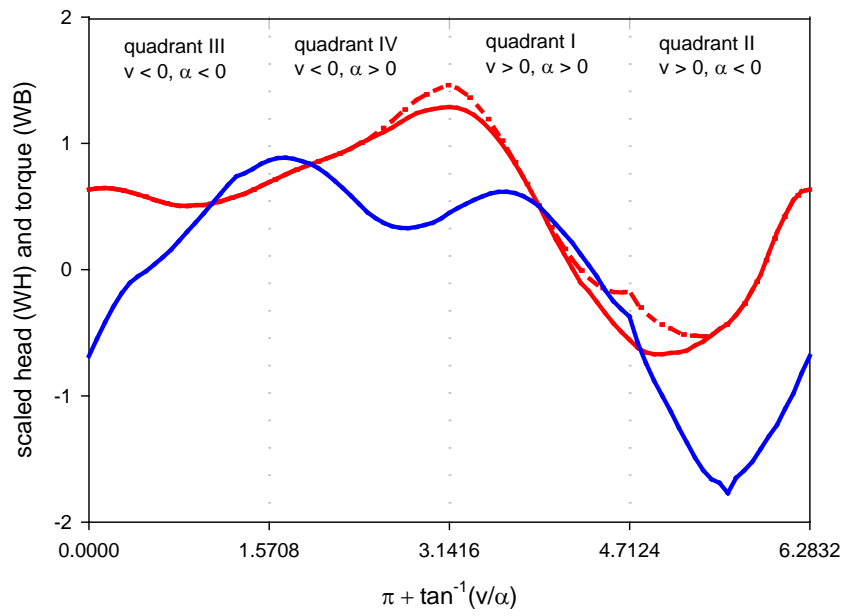
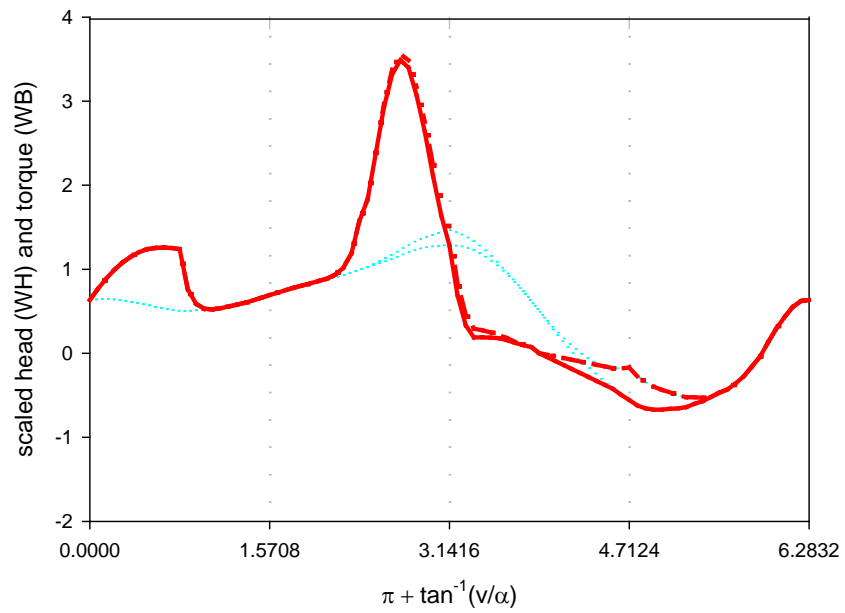Figure 11 Estimated four quadrant head and torque curves for 3 hp and ½ hp pumps

Figure 12 Estimated four quadrant head curves degraded by entrained air and vapor

22

In modeling, the modified head curve and torque curve in Figure 11 are used in the steady-state. During transients, if the pressure at pump suction is above its steady-state value, the modified head curve is used again. If the pressure lies between its steady-state value and the water's vapor pressure, a linear interpolation is made between the modified and the degraded curves. For air vent tests, the degraded head curve alone is used after the vent opens.

There are six variables involved in pump modeling: (1) head at pump suction H_s; (2) head at pump discharge H_d; (3) flow through the pump Q; (4) total dynamic head produced by the pump TDH; (5) resistive torque T; and (6) pump rotational speed ω. The available equations are:

(1) The scaled pump head versus scaled flow relationship represented by the *WH* curve

(2) The scaled pump torque versus scaled flow relationship represented by the *WB* curve

(3) The energy balance across the pump:

$$H_d - H_s = TDH \tag{12}$$

(4) The C+ compatibility equation from the suction pipe:

$$H_s = CP - BP\,Q \tag{13}$$

(5) The C- compatibility equation from the discharge pipe:

$$H_d = CM + BM\,Q \tag{14}$$

(6) The relationship between rotational acceleration and the applied resistive torque:

$$T = \frac{-WRR}{g}\frac{d\omega}{dt} \tag{15}$$

In the above, *CP*, *BP*, *CM*, and *BM* are constants representing the characteristic impedance and friction of the suction and discharge pipes. g = gravitational acceleration, and t = time.

8. Modeling the Air Vent

The other means to release vacuum at the sump is to open an air vent near the pump suction. The action and effect of the air vent will be modeled as an orifice. The air entered into the pipe

will be lumped at a computational section. The variables involved are: (1) mass flow rate of air *mdot*; (2) absolute pressure inside pipe and at the computational section P; (3) flow toward the computational section QU; (4) flow moving away from the computational section Q; and (5) head at the computational section H. The available equations are:

(1) The mass flow rate through the orifice. There are four possibilities:

(a) Subsonic air inflow:

$$mdot = CA_{in}\sqrt{7P_0\rho_0\left[\left(\frac{P}{P_0}\right)^{1.4286} - \left(\frac{P}{P_0}\right)^{1.714}\right]} \quad \text{if } P_0 > P > 0.53\,P_0 \tag{16}$$

(b) Sonic inflow:

$$mdot = CA_{in}\frac{0.686}{\sqrt{R\,T_0}}\,P_0 \quad \text{if } P \le 0.53\,P_0 \tag{17}$$

(c) Subsonic outflow:

$$mdot = -CA_{out}\sqrt{\frac{7}{R\,T}\left[\left(\frac{P_0}{P}\right)^{1.4286} - \left(\frac{P_0}{P}\right)^{1.714}\right]} \quad \text{if } \frac{P_0}{0.53} > P > P_0 \tag{18}$$

(d) Sonic outflow:

$$mdot = -CA_{out}\frac{0.686}{\sqrt{R\,T}}\,P \quad \text{if } P > \frac{P_0}{0.53} \tag{19}$$

In the above, CA_{in} = product of discharge coefficient C and orifice cross-sectional area A for inflow, CA_{out} = product of C and A for outflow, R = the gas constant of air, T_0 = absolute air temperature outside pipe, T = absolute air temperature inside pipe, P_0 = absolute pressure outside pipe. Values for CA_{in} and CA_{out} need to be established from tests.

(2) The C+ compatibility equation from the pipe segment upstream of the orifice:

$$H = CP - BP\,QU \tag{20}$$

(3) The C- compatibility equation from the pipe segment downstream from the orifice:

$$H = CM + BM\,Q \tag{21}$$

(4) The equation of state for the air mass inside pipe:

$$P \left\{ V_{aold} + \frac{dt}{2} [\, (Q - QU) + (Q_{old} - QU_{old}] \right\} = \left[m_{old} + \frac{dt}{2} (mdot + mdit_{old}) \right] R\,T$$

(22)

(5) The absolute pressure - head relationship at the section:

$$P = \gamma(H - \beta)$$

(23)

9. Modeling a Dual-Drain

An effective way to prevent vacuum from developing is to use dual drains. When the first drain is blocked suddenly, the low pressure induced in the suction pipe will cause an inrush of flow from the second drain, which can release the vacuum at the first. The dual drain configuration indicated in Figure 1 is modeled by adding a "T" junction to the system model and by adding a second drain that remains fully open.

In modeling the "T" junction, head losses at the junction are ignored. There are four variables: (1) junction head H; (2) flow into junction from the first drain $Q1$; (3) flow into junction from the second drain $Q2$; and (4) flow leaving the junction $Q3$. The available equations are:

(1) The C+ compatibility equation from the pipe between the first drain and the junction:

$$H = CP1 - BP1\,Q1$$

(24)

(2) The C+ compatibility equation from the pipe between the second drain and the junction:

$$H = CP2 - BP2\,Q2$$

(25)

(3) The C- compatibility equation from the suction pipe downstream of the junction:

$$H = CM + BM\,Q3$$

(26)

(4) The continuity equation:

$$Q1 + Q2 = Q3$$

(27)

The variables for the second drain sump are: (1) head in the drain sump H_s; (2) head in the inlet of the pipe between the drain and the junction H; and (3) flow into the pipe Q. The applicable equations are:

(1) The C- compatibility equation from the pipe between the drain and the junction:

$$H = CM + BM \, Q \tag{28}$$

(2) Relationship between pool head and sump head (applicable to both sumps):

$$H_{pool} = H_s + (1 + K_0)\frac{Q^2}{2g \, A_s{}^2} \quad if \; Q > 0 \tag{29}$$

$$H_{pool} = H_s \quad if \; Q \leq 0 \tag{30}$$

(3) Relationship between sump head and suction pipe inlet head (applicable to both sumps):

$$H_s = H + (1 + K_0)\frac{Q^2}{2g \, A_s{}^2} \quad if \; Q > 0 \tag{31}$$

$$H_s = H \quad if \; Q \leq 0 \tag{32}$$

10. Modeling Transients in Pipes

Because the drain line is a low-head system, it is very likely that the water contains some free air (as opposed to dissolved air in the water). It is also very likely that some free air may be entrapped in piping at the numerous turns and elbows. To allow for the free air, the discrete gas cavity model (Wylie 1984, Liou 2000) is used. In this model, some fixed amount of free air is assumed to exist and the wave speeds are pressure-dependent. In the model, the air mass is lumped at the pipe interior computational sections. The water column between sections is regarded as free of air. This approach allows the well-established method of characteristics with constant wave speed (Wylie and Streeter 1993) to be used. The model allows gaseous vapor cavities to form, grow, and collapse in the pipe interior. It was found to be essential to include free air in modeling SVRS.

In capturing the frictional resistance to flow by the pipes, an absolute roughness of zero was assumed for the PVC pipes. Steady-state friction factors established from the Moody diagram with the applicable Reynolds numbers were used during transients.

There are four variables at the computational section: (1) head at the section; (2) flow toward the section; (3) flow leaving the section; and (4) the absolute pressure at the section. The available equations are:

(1) The C+ compatibility equation from the upstream pipe segment:

$$H = CP - BP\ QU \tag{33}$$

(2) The C- compatibility equation from the downstream pipe segment:

$$H = CM + BM\ Q \tag{34}$$

(3) The equation of state for the air mass at the section:

$$P \left\{ V_{aold} + \frac{dt}{2} [\ (Q - QU) + (Q_{old} - QU_{old}] \right\} = m\ R\ T \tag{35}$$

(4) The absolute pressure - head relationship at the section:

$$P = \gamma(H - \beta) \tag{36}$$

11. Modeling the Complete System

All the components described above are integrated into an interconnected system by the C+ and C- compatibility equations. The method of characteristics with a fixed time interval is used. The pipes are divided into computational reaches with equal length of one foot. The time step size is governed by the Courant condition

$$dt = \frac{dx}{a} \tag{37}$$

in which dx = computational reach length and a is the water hammer wave speed in the system. The wave speed for a 2-inch schedule 40 PVC pipe containing water free of free air is estimated at 1450 ft/s. The numerous elbows in the system may have made the pipe stronger (*i.e.*, higher wave speed). On the other hand, the presence of free air (as opposed to dissolved air) in the water significantly lowers the wave speed. In low-pressure systems with numerous fittings (valves and elbows), such as the test facility, it is highly likely that free air was present in the system. And it is not possible to quantify the mass and location of such free air in the system. Consequently, the wave speed cannot be determined a priori.

12. Additional Uncertainties and Assumptions

As described previously, there are one control valve and nine elbows on the suction piping and three control valves and 16 elbows on the discharge piping. The control valve on the suction-side control valve was kept wide open and incurred no head loss. On the discharge side, control valves were throttled equally to obtain the desired steady-state flow rate. The head loss coefficients of the elbows and valves were unknown. Separately, the rated conditions of the pumps are also unknown. In the Interim Report (Liou 2009), and for each test, the measured steady-state pressures at Pu, Ps, Pd, and Pvid were used to estimate the head loss coefficients of the elbows and the throttling valves and the rated head of the pumps. This process is cumbersome and questionable because the rated head of the pump should not vary from test to test. In the simulations reported here, an elbow head loss coefficient of unity is assumed.   The rated heads of the pumps were assumed so that, in conjunction with the assumed rated flows and known pump speed (3450 rpm), a specific speed close to 1270 (in gpm units) was obtained. This specific speed represents a radial centrifugal pump, which is the case for the pumps used. In addition, the four-quadrant performance data for a centrifugal pump with a specific speed of 1270 are known and adopted for this study. With the elbow head loss coefficients and the rated head of the pumps established, the head loss coefficients for the control valves were computed based on an overall steady-state head balance.

Free air, either entrapped in the piping or entrained by the flow, influences the dynamic behavior of SVRS.   A very small amount of free air will significantly influence the transient hydraulics in SVRS. In modeling, a fixed amount of free air is assigned at the sump and at the computational sections to account for the effect of free air (Wylie 1984, Liou 2000). Because it was impossible to measure the amount of free air during tests, the amount of free air was estimated by trial and error until a reasonable match between the simulated and the measured pressure traces was obtained. In terms of void fraction at atmospheric pressure, the amount of free air so determined is 0.0017 for the piping, 0.005 for the sump during pump switch tests (Cases 1 to 5), and 0.0005 for the air vent tests (Cases 6 to 11).

In air vent modeling, a value of 0.12 was used for the discharge coefficient *C.* This value is selected so that the model can distinguish tests with blocker release from tests without. This coefficient is small compared with 0.6 for an ideal sharp-edged orifice during steady flow. Since the air inflow starts impulsively and since the flow path is somewhat obstructed during inflow, a value of 0.12 is considered plausible.   The air entered into the pipe is assumed to be gathered at the computational section where the air vent is connected to.   Should the pipe exceed atmospheric pressure later, air will be expelled through the vent.

13. Single-Drain Modeling Results and Comparison with Measurements

The simulated pressures and pump speed for pump switch tests are compared with the measured data in Figures 13 through 17. For air vent tests, the pump speed is known and fixed. Only the simulated and measured pressure traces are compared. These are shown in Figures 18 through 27.   A running average of 10 data points were used in presenting the measured data.   In the simulations, because the time step used is very small (0.00069 seconds), and because the need to keep a large amount of data in memory for animations, only one of every 10 consecutive points was saved and plotted in the simulated results.   No details are lost because of this. However, spikes may appear in the simulations but not in the plots of measured data.

Differentiating features were captured between tests with different parameters, such as mode of vacuum release (pump switch versus air vent), pump horsepower, suction pipe length, pump elevation, steady-state flow rate, and orifice size of the air vent. Uncertainties in the amount and location of free air and in the pump characteristics and its moment of inertia prevented a better match between simulation and measurements. It is interesting to note that Cases 9-1 and 9-2 are borderline (release or no release) tests with the same test configurations.

Of particular interest in the simulated results is the vacuum release time. A comparison is shown in Table 5. Despite the uncertainties, the model can predict the vacuum release time reasonably well under different tests conditions. It is interesting to note that Cases 9-1 and 9-2 are tests conducted in research for the border between release and no release. For these cases, the simulations showed two or three "bounces" in the Pu pressure trace before release occurred, suggesting that these tests were close to the border between release and no release. The peaks associated with the peaks in Pu are shown in Table 5.

Additional plots are used to understand the SVRS transients. The top panel of Figure 28 shows the inflow (flow entering the drain sump) and outflow (flow returning to the tank) over time for pump switch Case 3. At the moment of drain blockage, tb, the inflow reduced rapidly, but not instantaneously, due to the volumetric flux of the foam blocker. The time lag in the outflow reduction is due to the fact that it takes some time for the pressure and flow waves to reach the pipe exit to the tank. The outflow started to reverse at about 1.6 seconds.   It is this reversed flow that eventually arrived at the sump, collapsed the cavity of vapor and air mixture (see bottom panel), and released the blocker. After the pump was switched off, both inflow and outflow trended toward zero because there was no longer any head to drive the flow. The

Table 5 Vacuum Release Times

	Measured (sec)	Simulated (sec)
Case 1	3.70	3.421
Case 2	6.05	4.996
Case 3	3.25	3.288
Case 4	2.38	2.000
Case 5	2.38	2.105
Case 6-1	3.403	3.162
Case 6-2	3.467	3.138
Case 7	No release	No release
Case 8	2.344	2.190
Case 9-1	No release	2.345/3.012
Case 9-2	2.356	2.262/2.929/3.492
Case 10-1	No release	No release
Case 10_2	No release	No release
Case11-1	2.267	2.233
Case11-2	2.277	2.217

middle panel shows the flow and the head across the pump. The inertia of the pump and motor kept the pump in forward rotation (see Figure 19) against the temporary reversed flow but trended toward zero as expected.

Figures 29 through 32 compare the behaviors for Cases 6-2, 10-2, and 11-1. The main difference between cases 6-2 and 10-2 is the length of the suction piping.   The difference between Cases 10-2 and 11-1 is the orifice size of the air vent. The flows into and out of the piping are shown in Figure 29. Unlike the pump switch cases, the sustained flow reversal (see top panel of Figure 28) did not occur due to the continued pumping (see Figure 30), although momentary flow reversal did occur for all cases. After four seconds, the inflow and outflow in the middle panel of Figure 29 hovered around zero, while the flows in the top and bottom panels were over 20 gpm. This pattern is consistent with the simulation outcome that the foam blocker was not released for Case 10-2 (the middle panel).   Comparison between the top and middle panels of Figure 31 shows that Case 6-2, with longer suction pipe, drew more air sooner from the vent, which led to the release of the blocker. Comparison between the middle and bottom panels (small versus large orifices) suggests that it is the time rate of volumetric air inflow (the slope of the blue traces around 2 seconds), not the total amount of air admitted, that determines whether release occurs. Figure 32 shows the working of the air vent
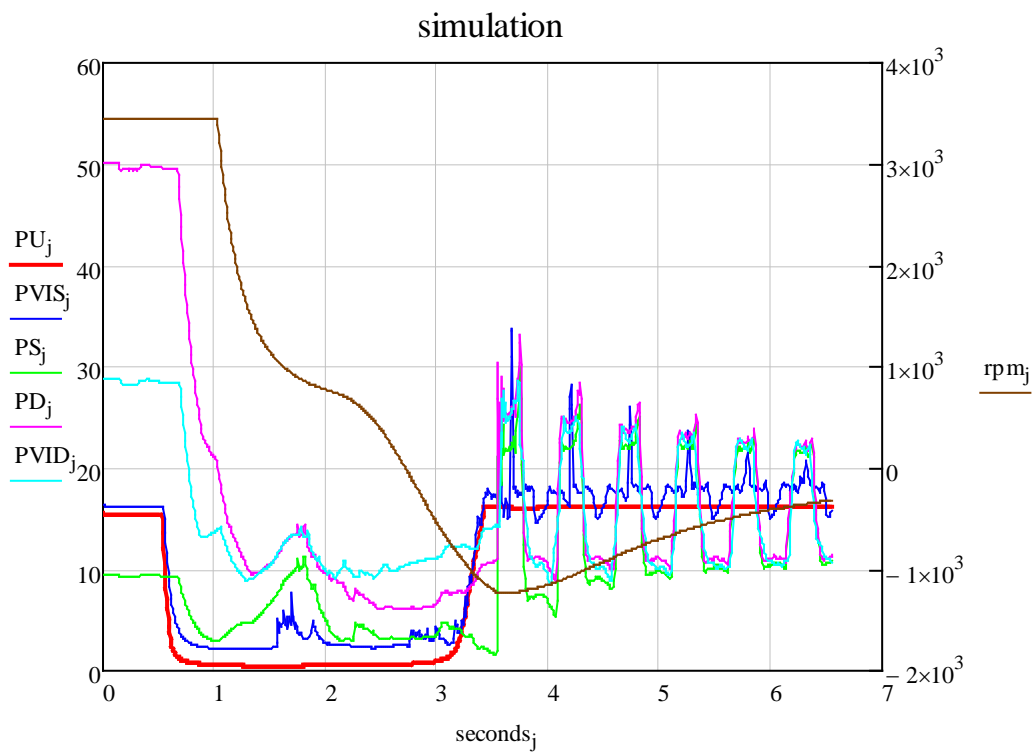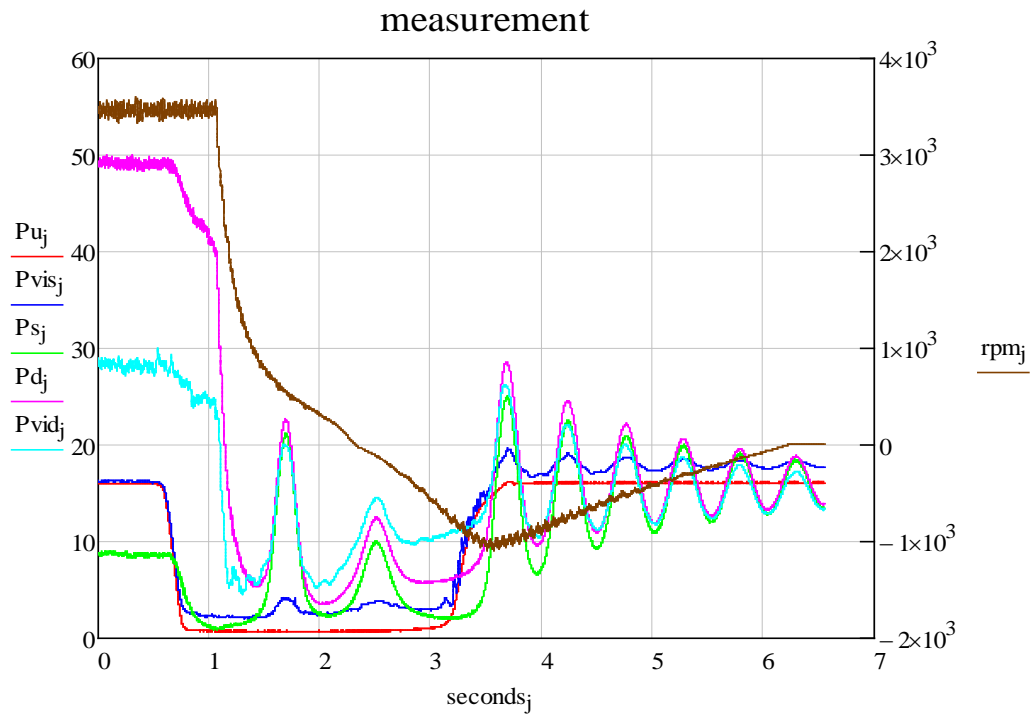
Figure 13 Case 1 comparison

measurement

simulation
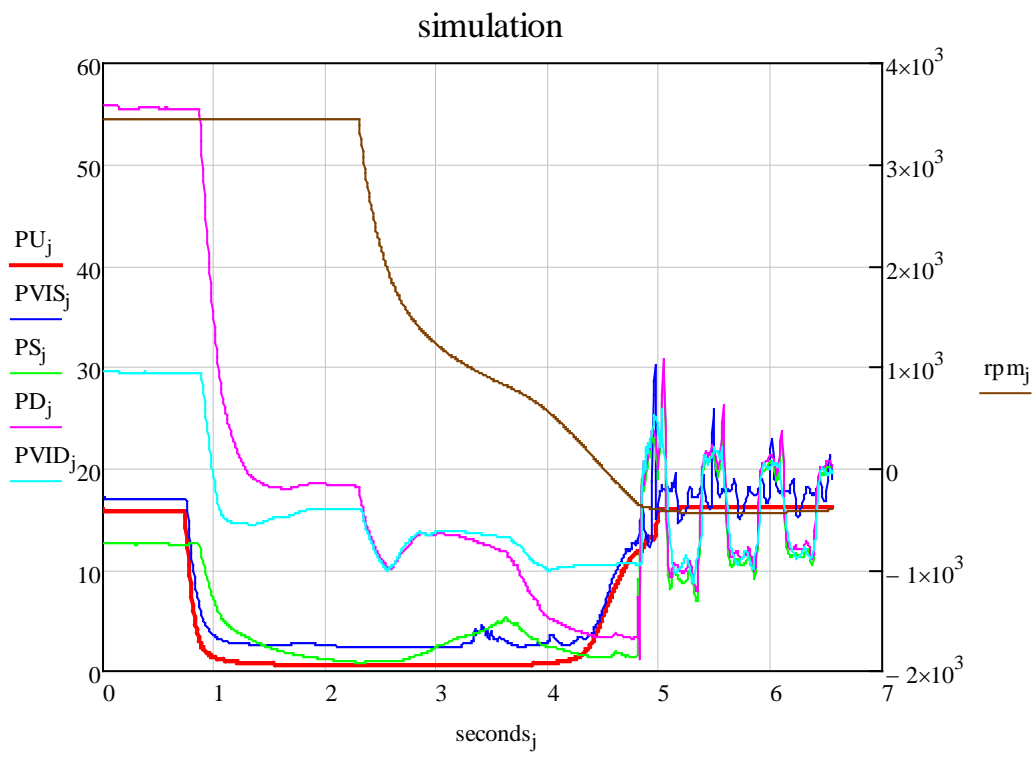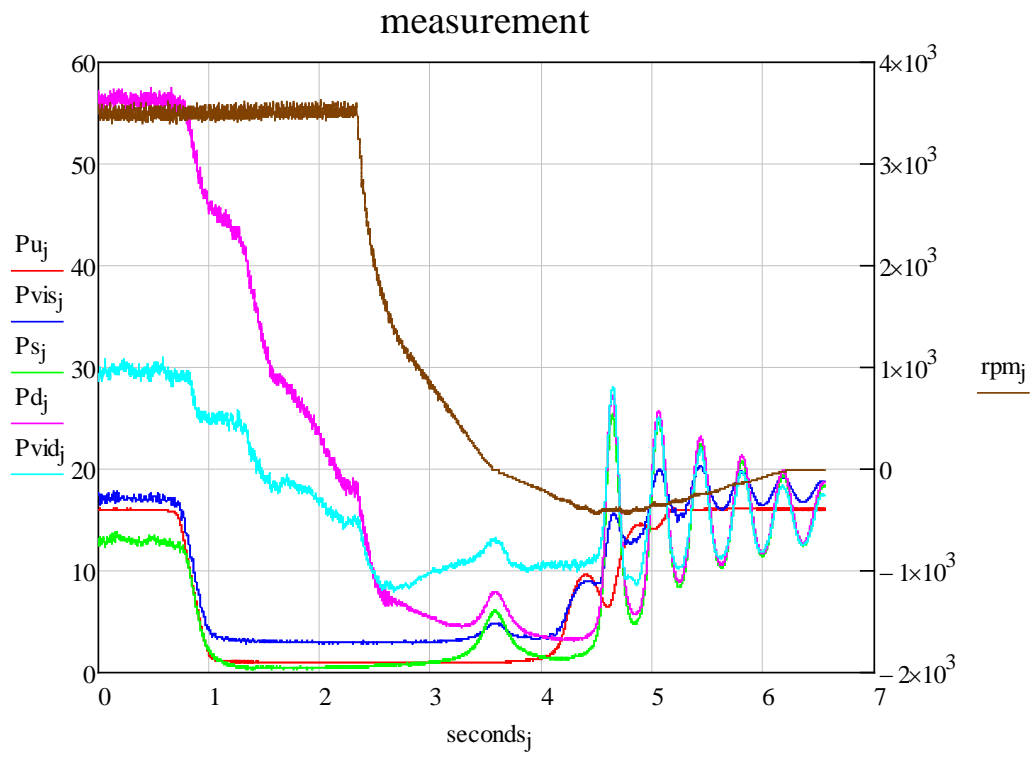
Figure 14 Case 2 comparison
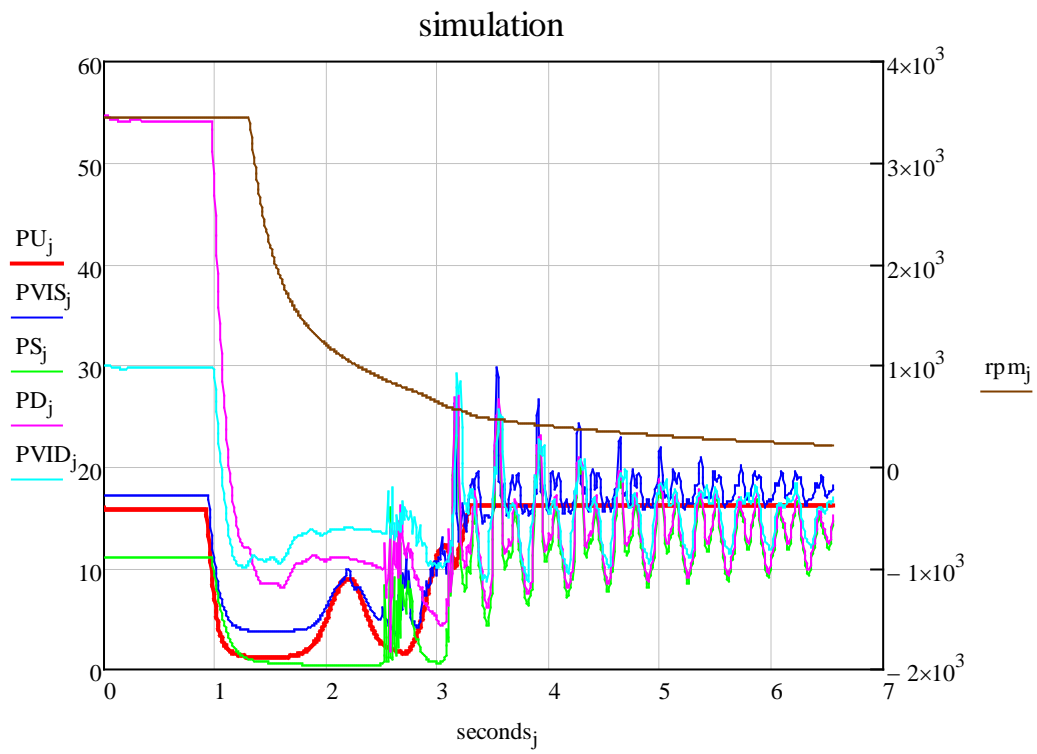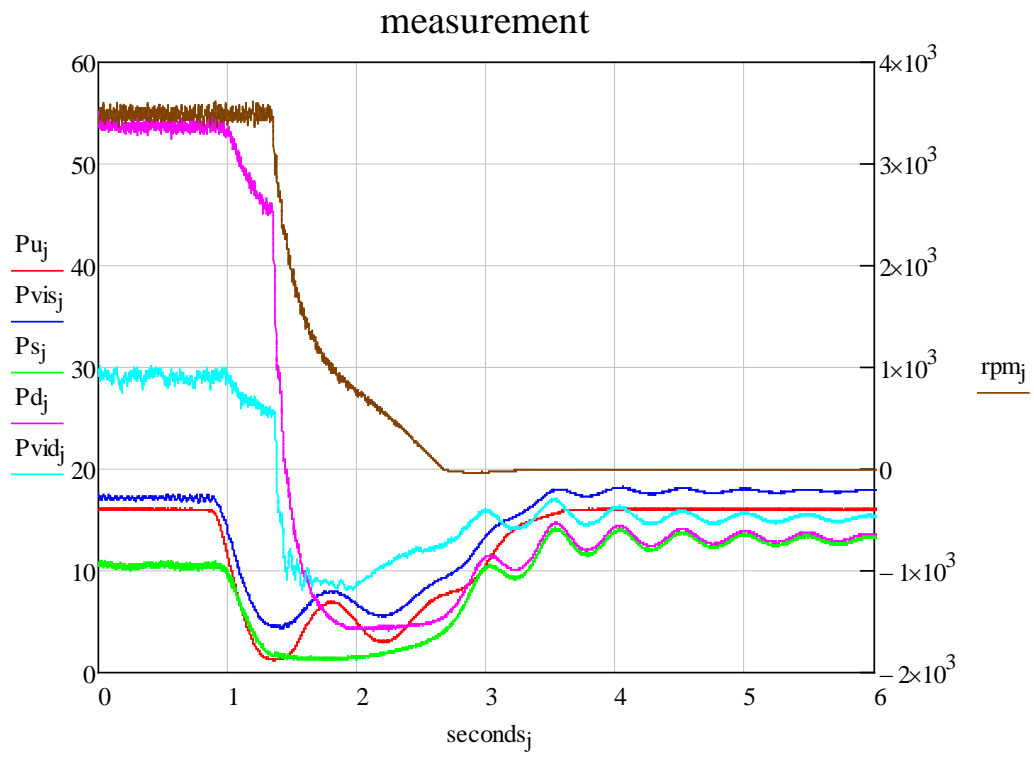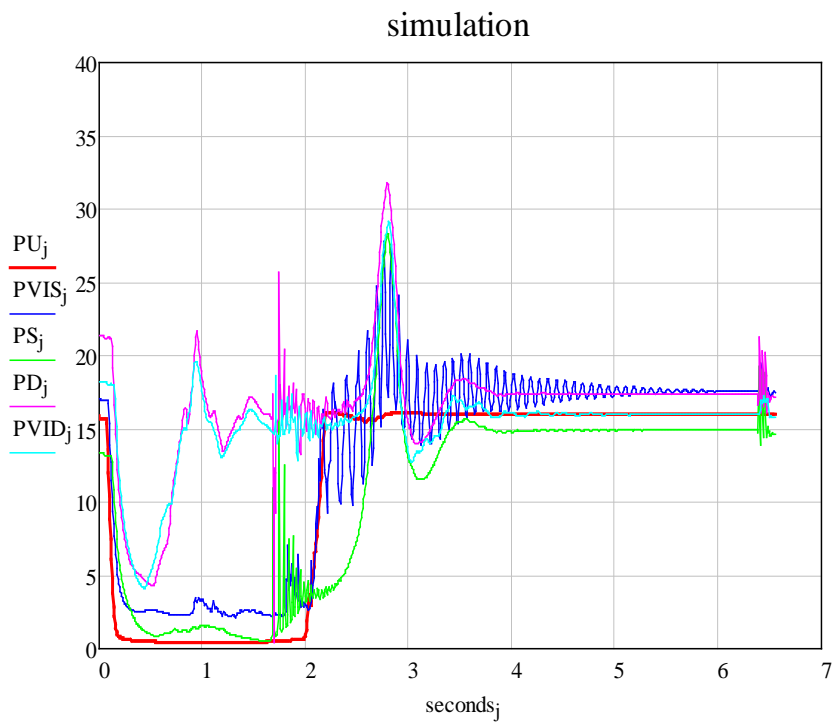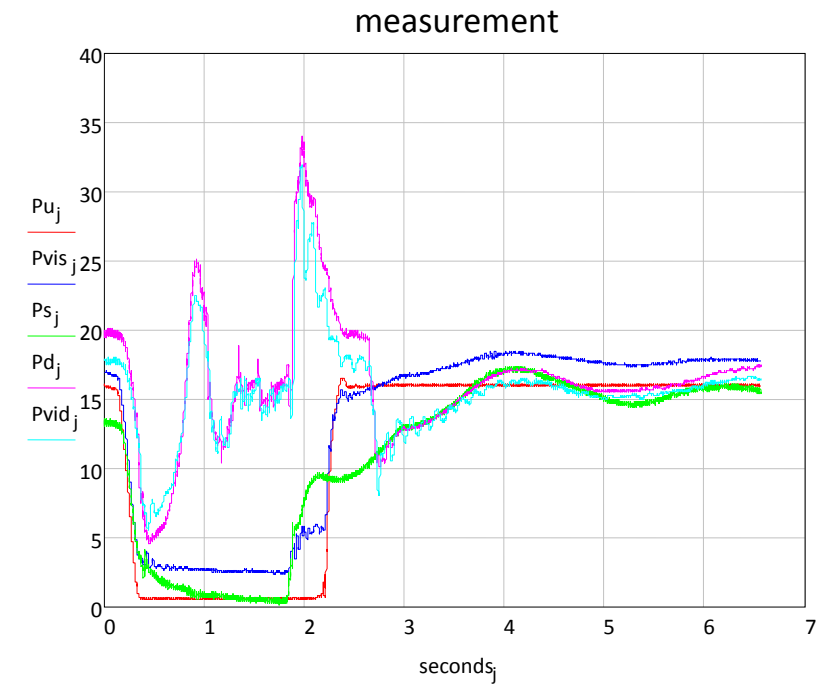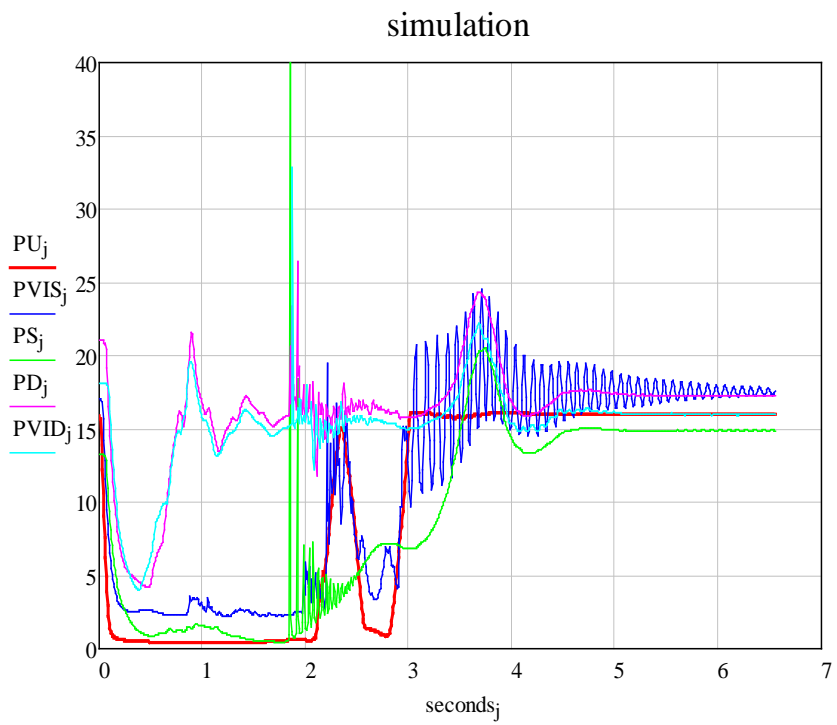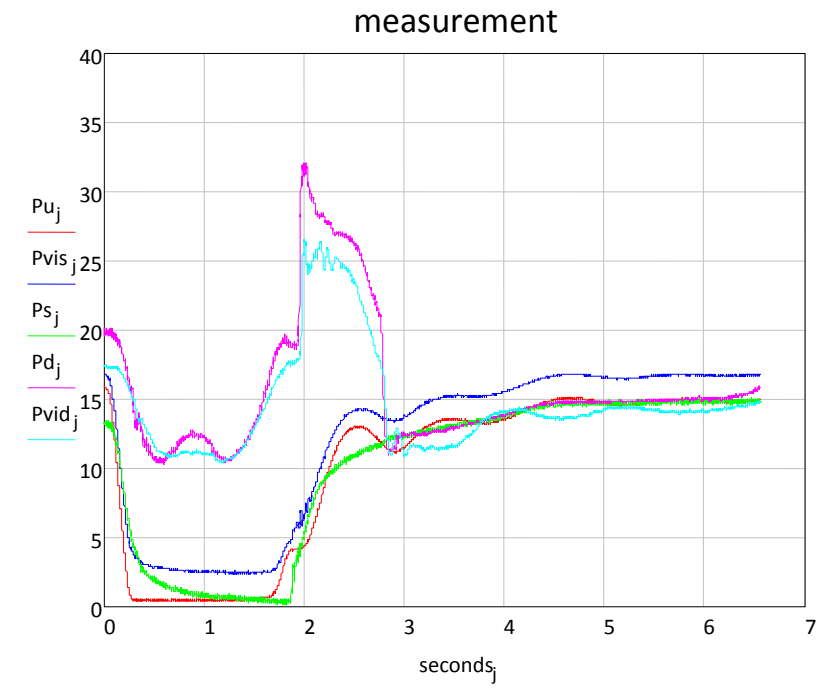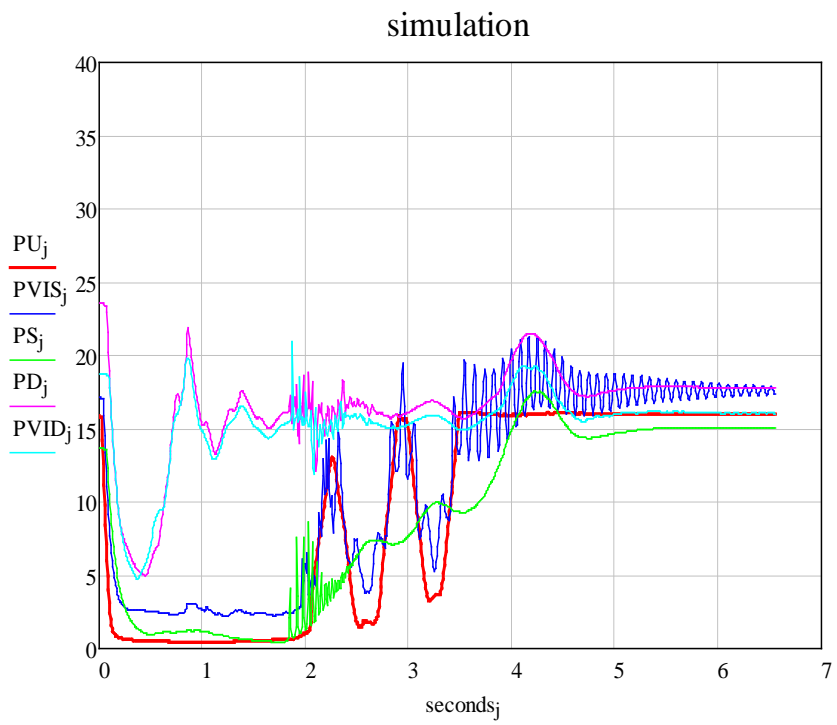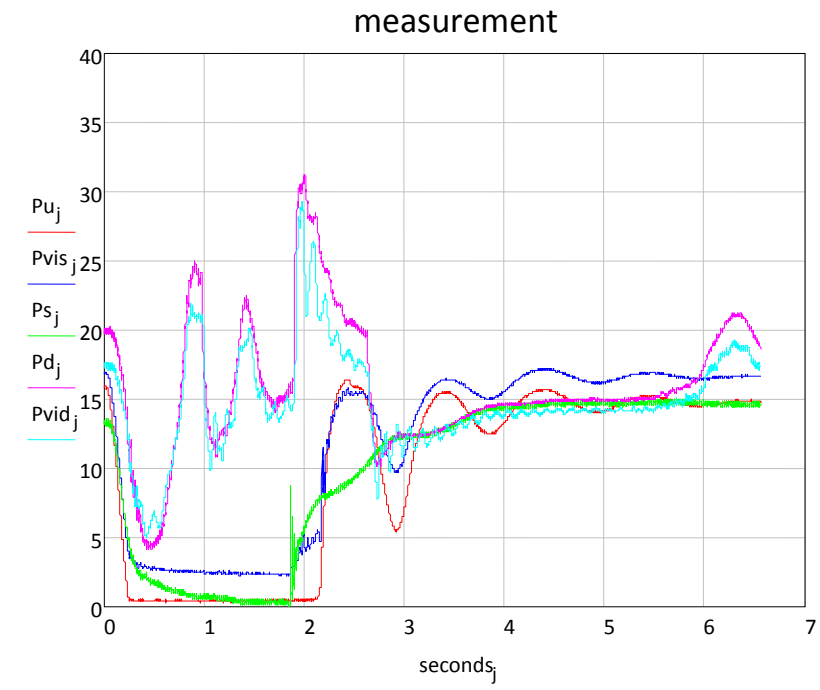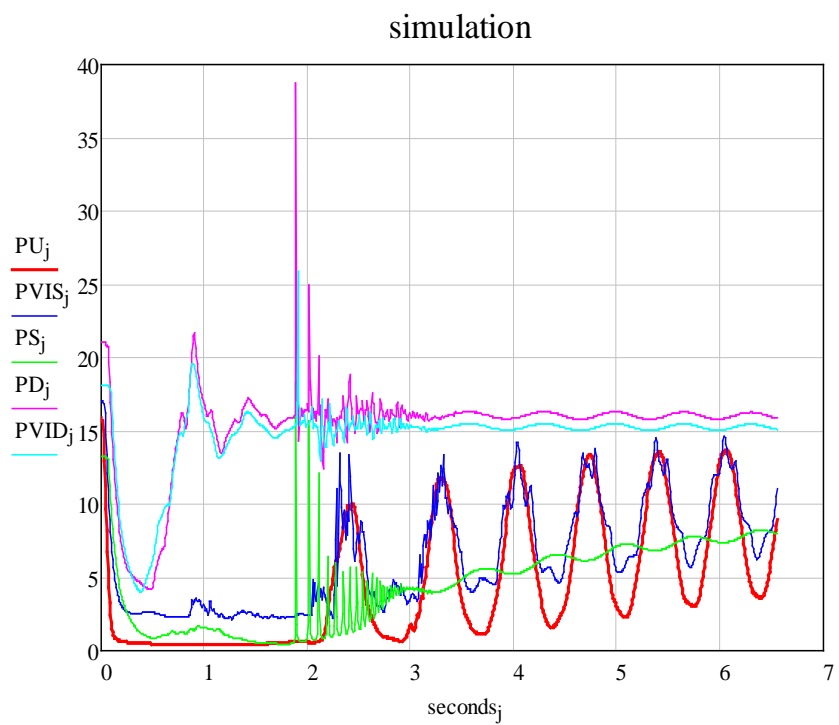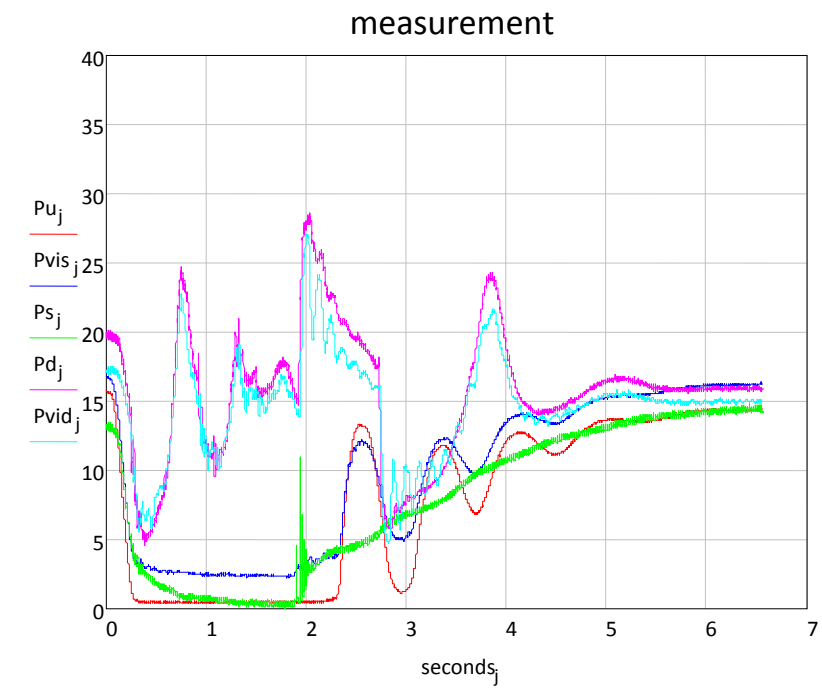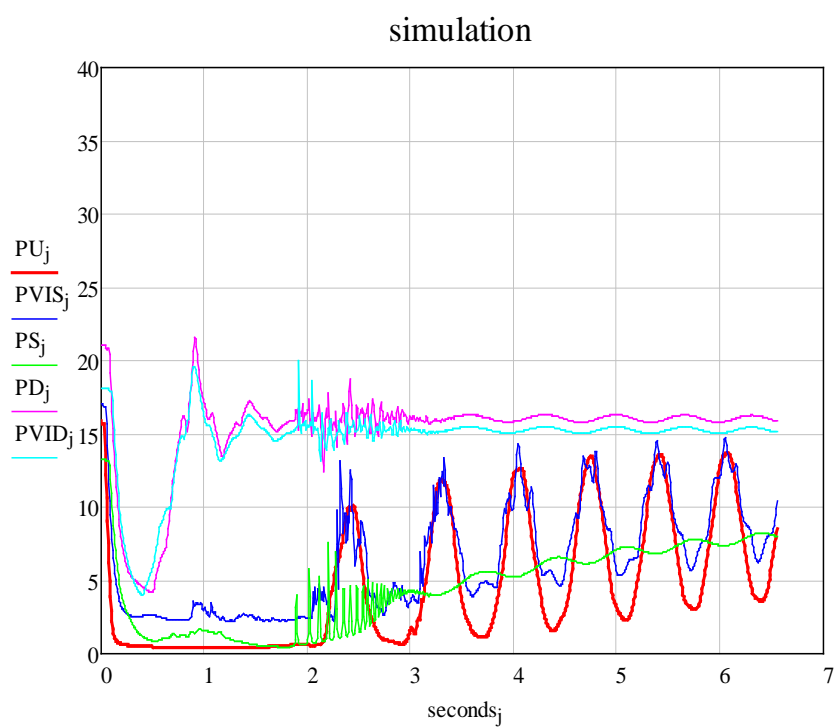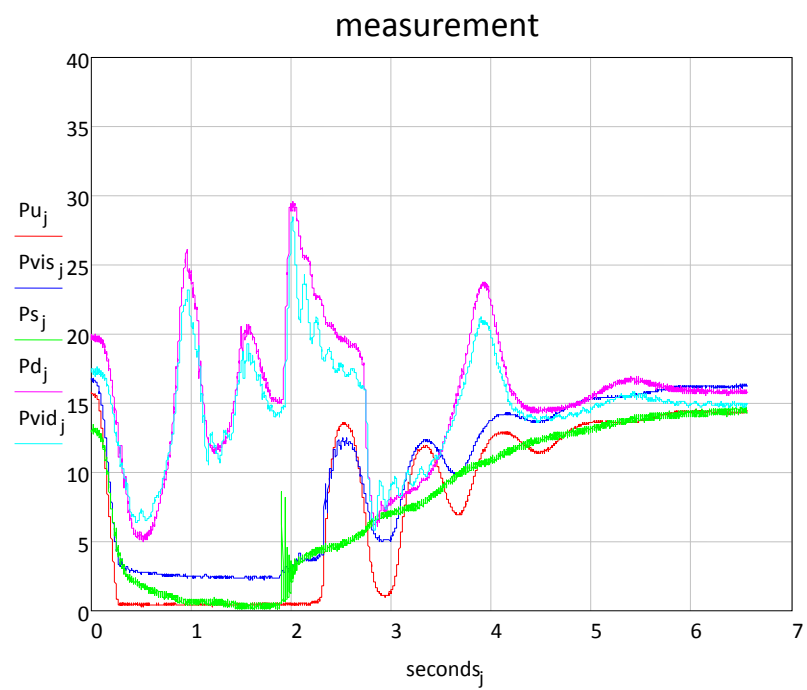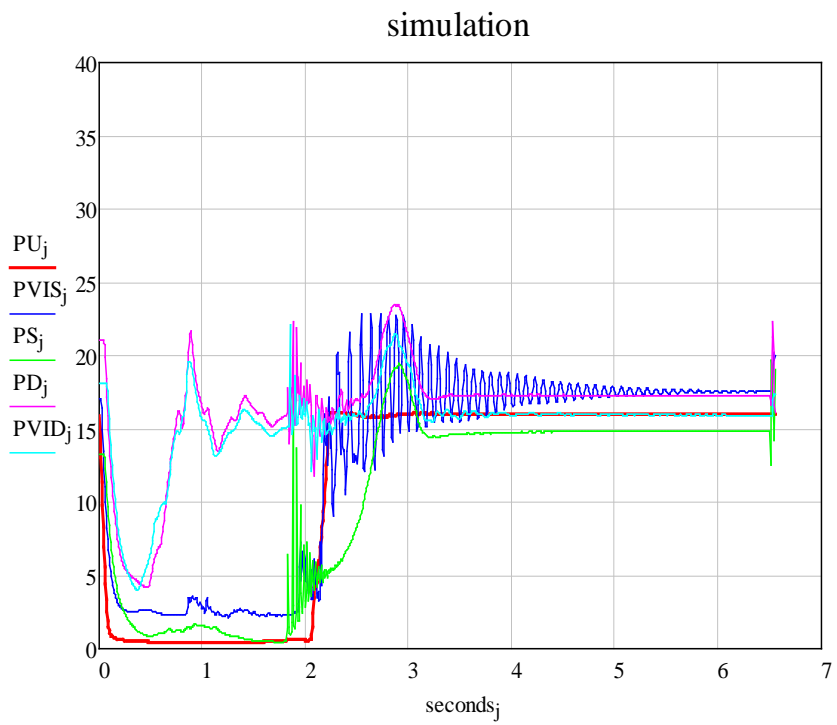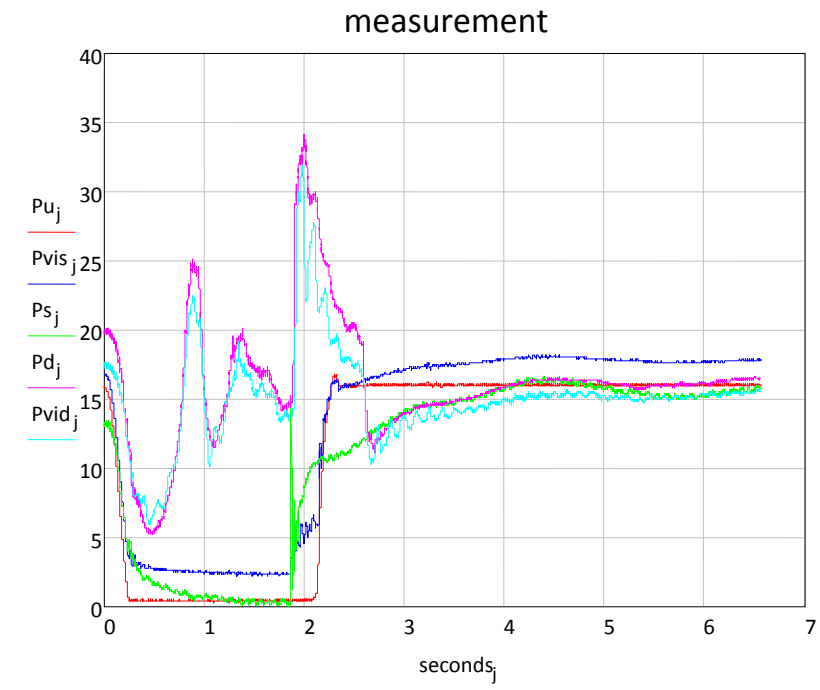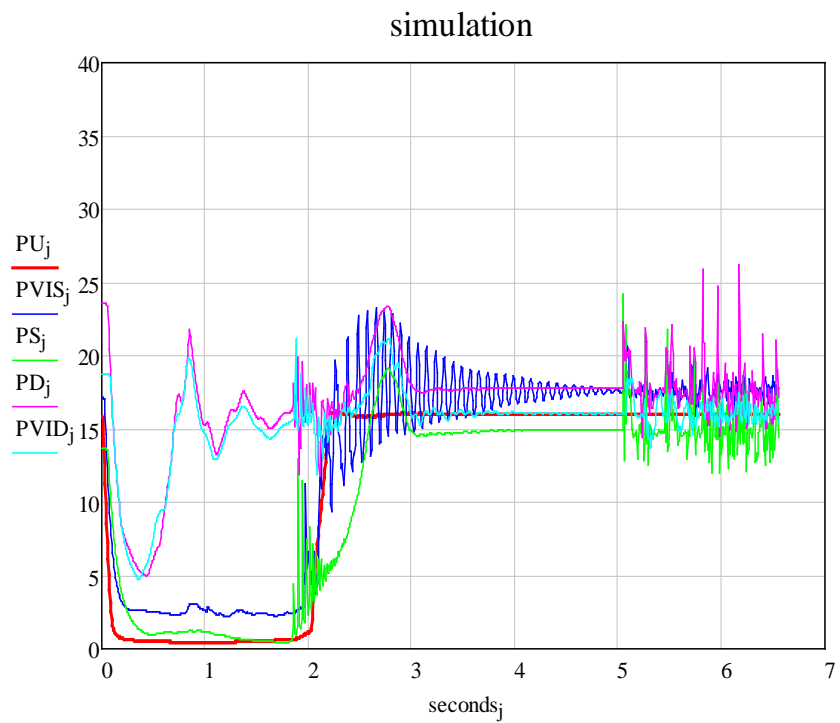
Figure 15 Case 3 comparison
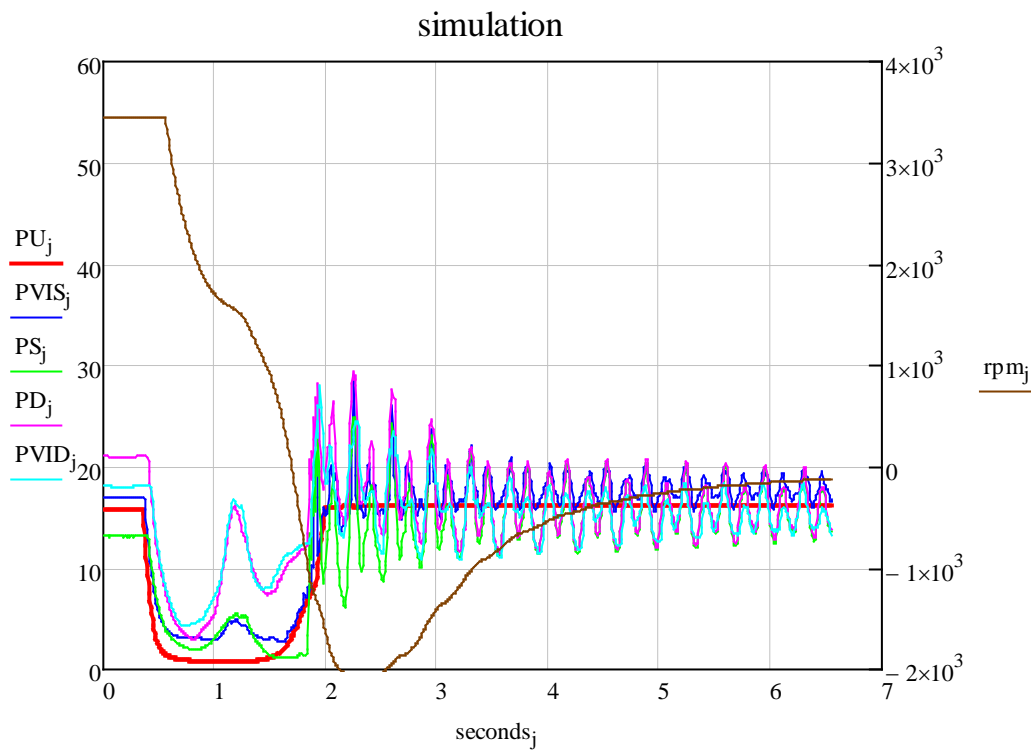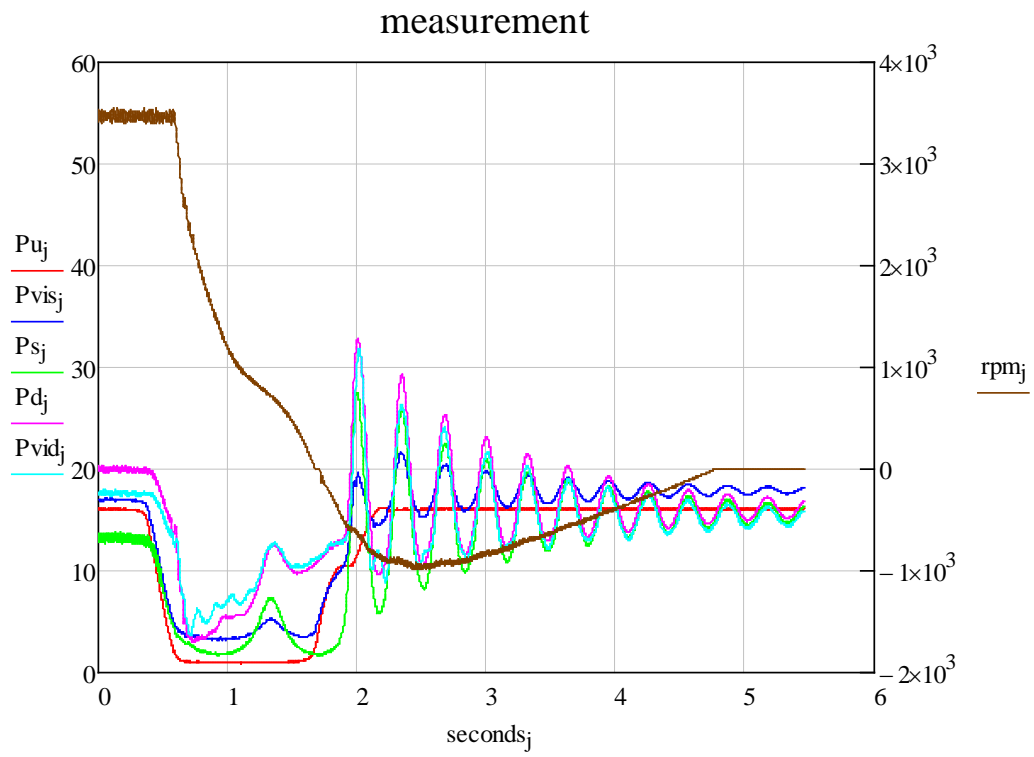
Figure 16 Case 4 comparison

34
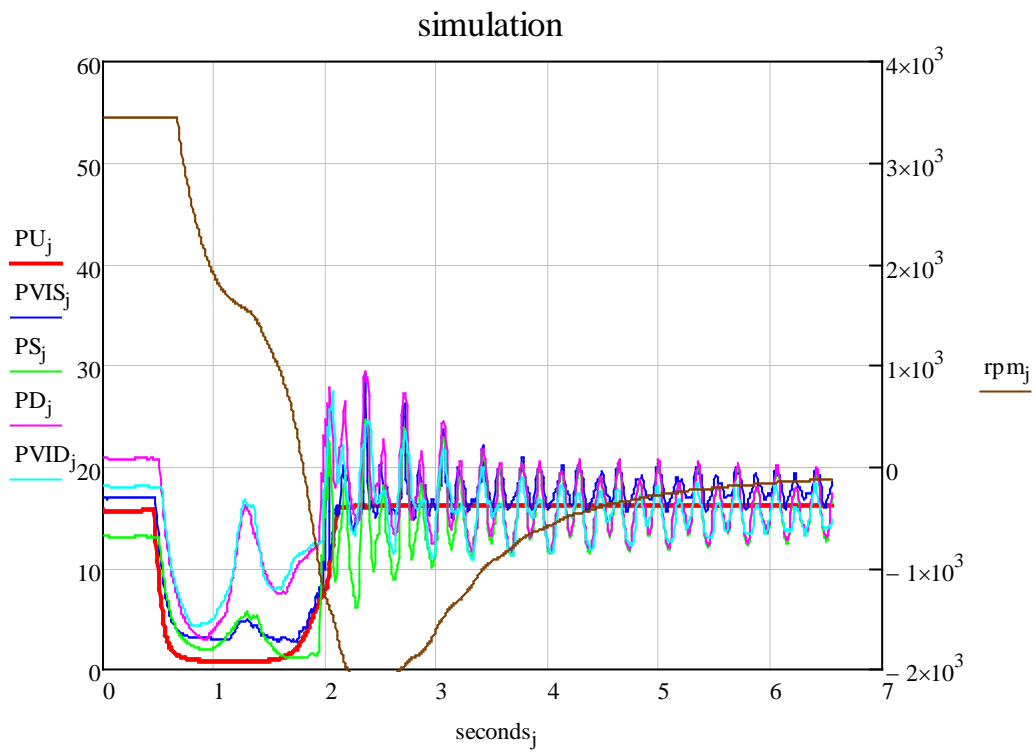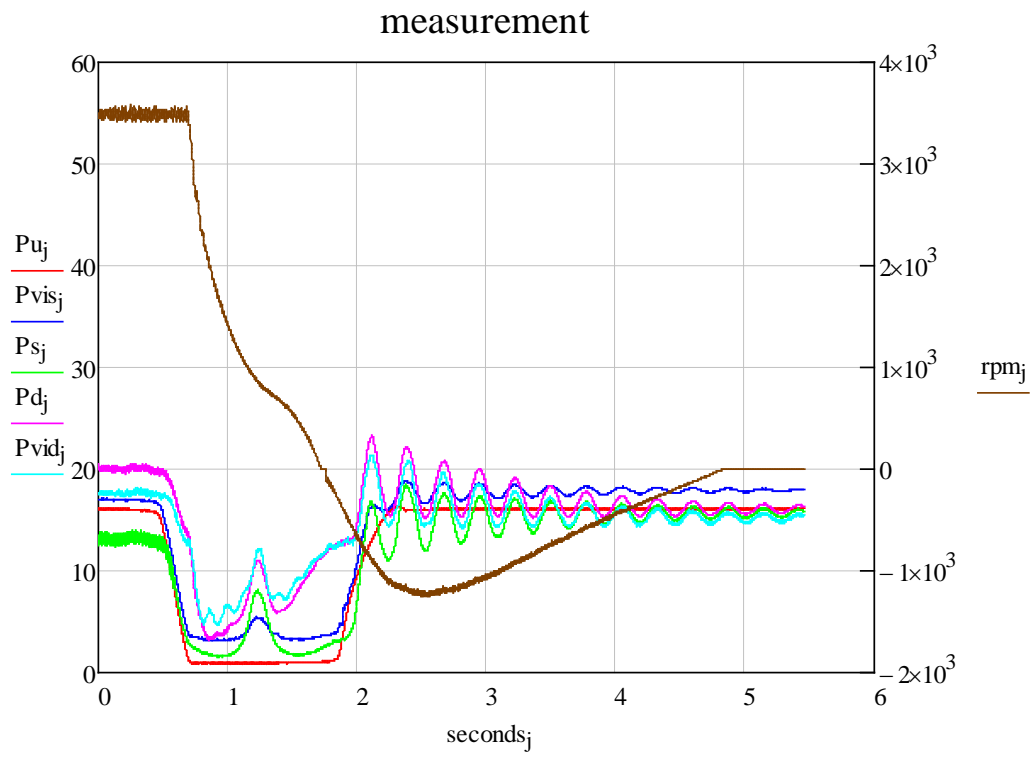
Figure 17 Case 5 comparison
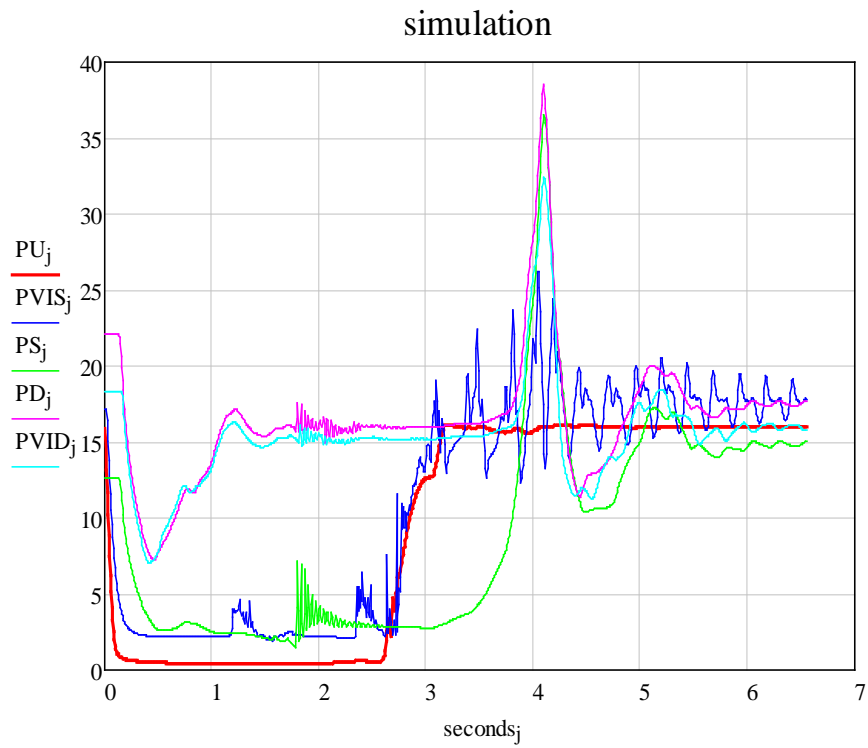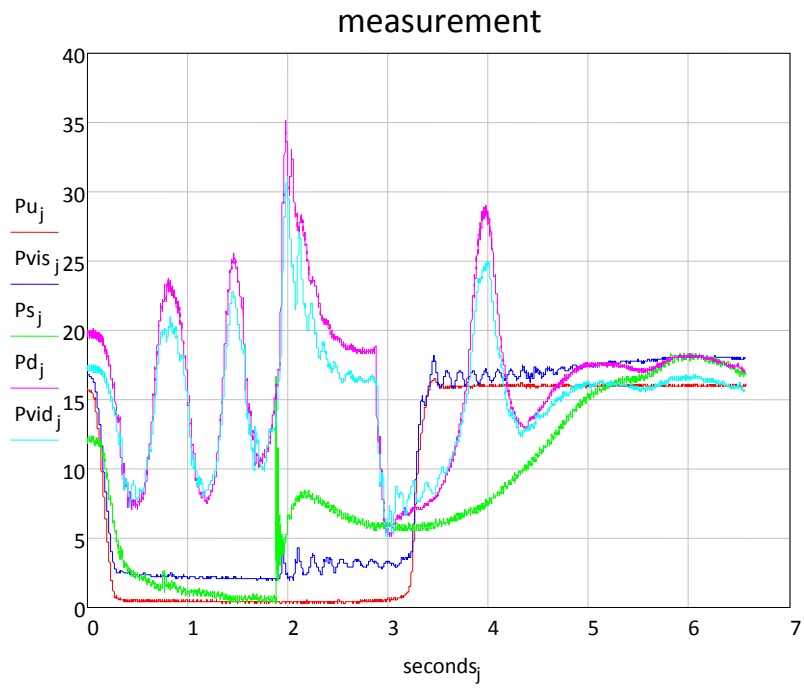
Figure 18 Case 6-1 comparison

measurement

simulation
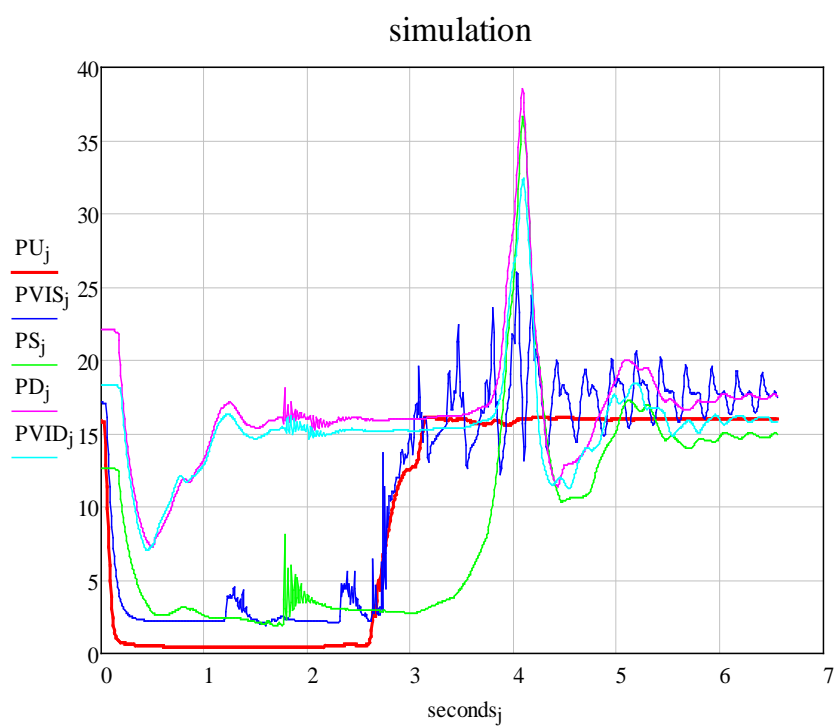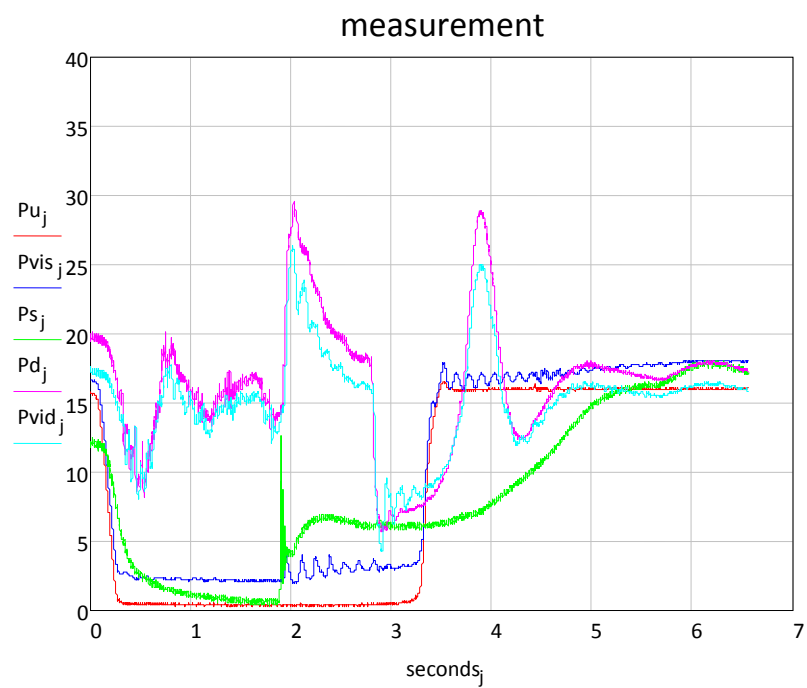
Figure 19 Case 6-2 comparison

37

measurement

simulation
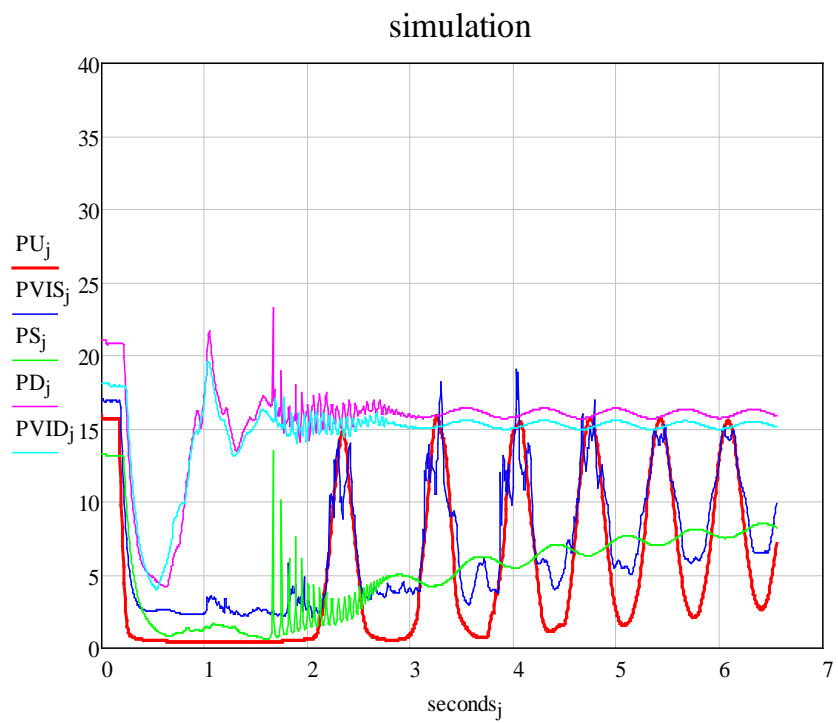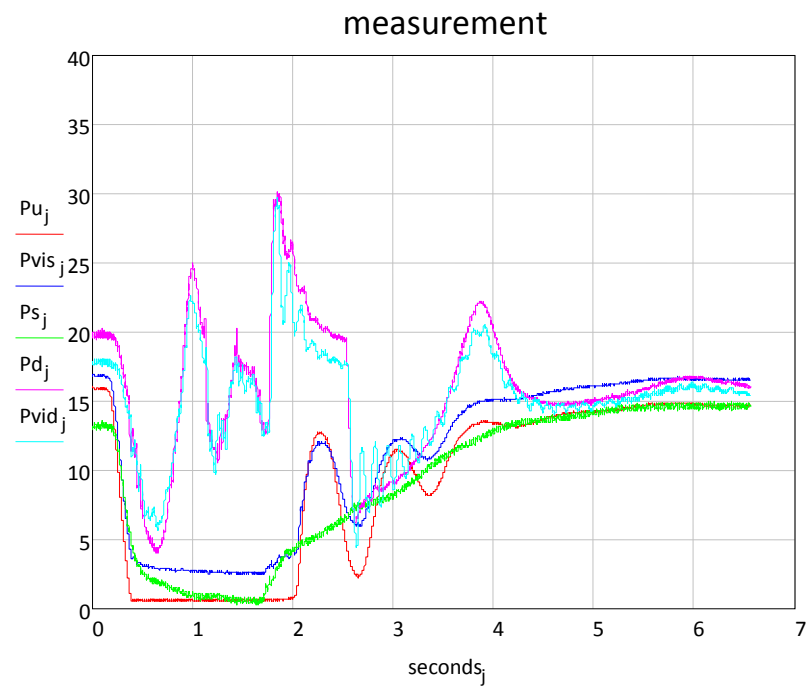
Figure 20 Case 7 comparison

38

measurement

Pu_j

Pvis_j

Ps_j

Pd_j

Pvid_j

seconds_j

simulation

PU_j

PVIS_j

PS_j

PD_j

PVID_j

seconds_j

Figure 21 Case 8 comparison

39

measurement

simulation

Figure 22 Case 9-1 comparison

measurement

Pu$_j$

Pvis$_j$

Ps$_j$

Pd$_j$

Pvid$_j$

seconds$_j$

simulation

PU$_j$

PVIS$_j$

PS$_j$

PD$_j$

PVID$_j$

seconds$_j$

Figure 23 Case 9-2 comparison

41

measurement

simulation

Figure 24 Case 10-1 comparison

42

measurement

simulation

Figure 25 Case 10-2 comparison

measurement

simulation

Figure 26 Case 11-1 comparison

44

measurement
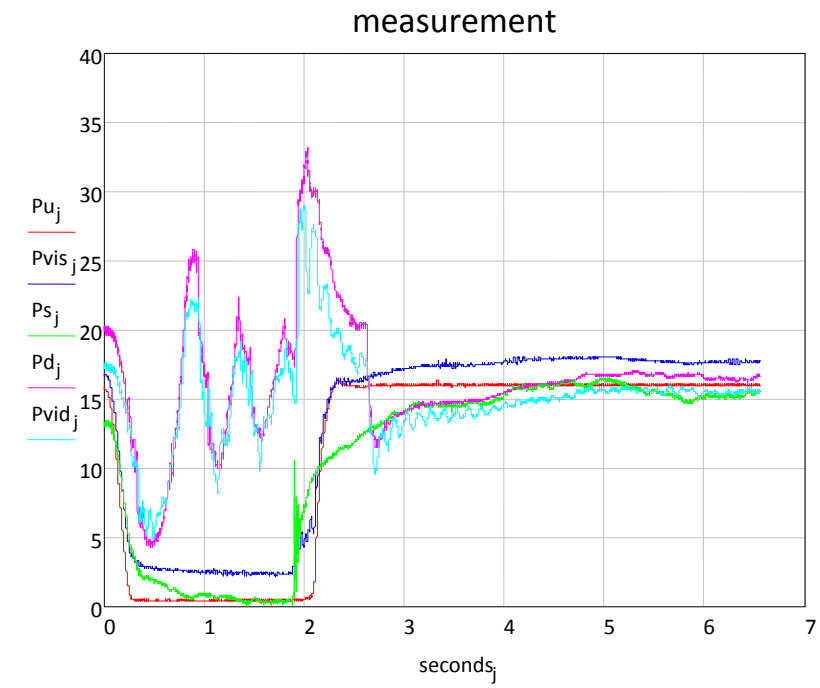
simulation

Figure 27 Case 11-2 comparison

45
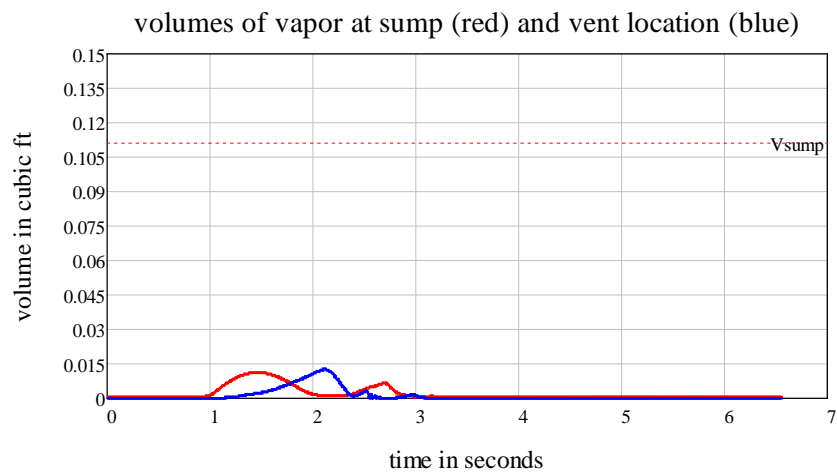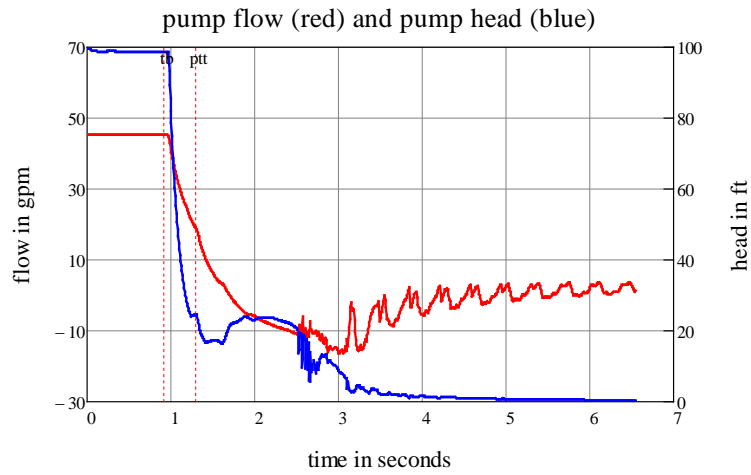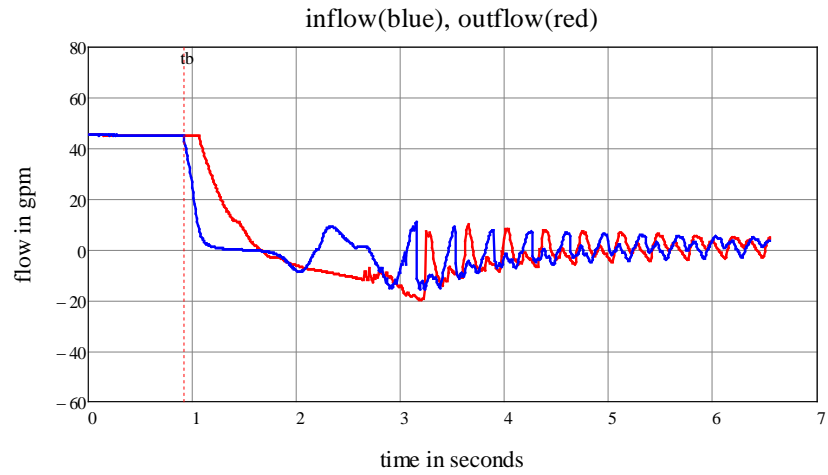
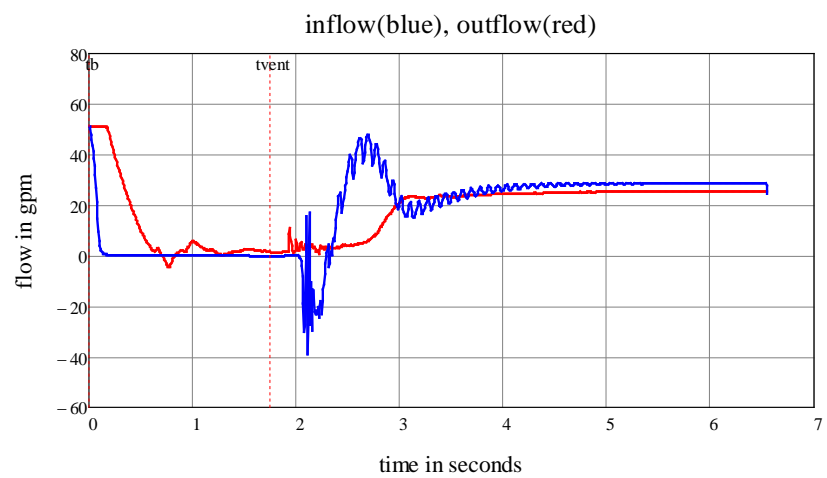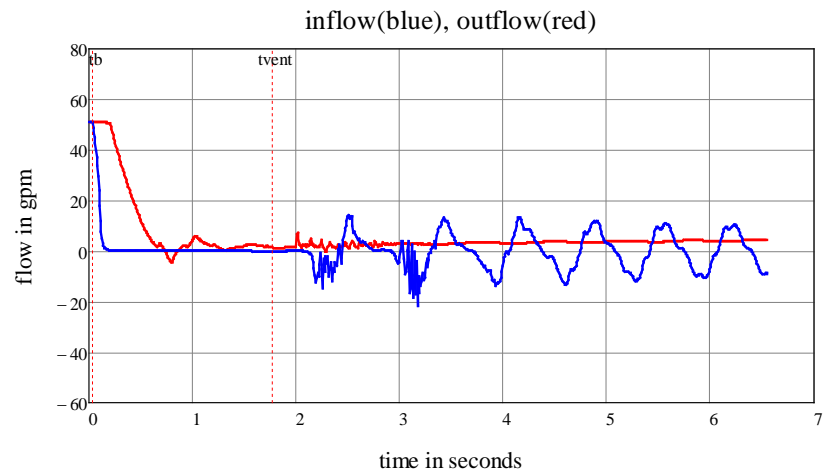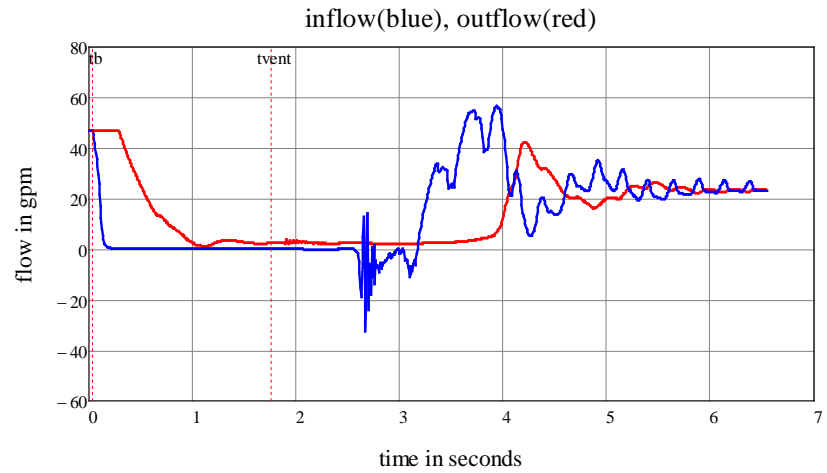Figure 28 Details for simulation case 3 showing overall flows, pump behavior, and cavity volumes

Figure 29 Comparison of inflow and outflow for simulation cases 6-2 (top), 10-2 (middle), and 11-1 (bottom)
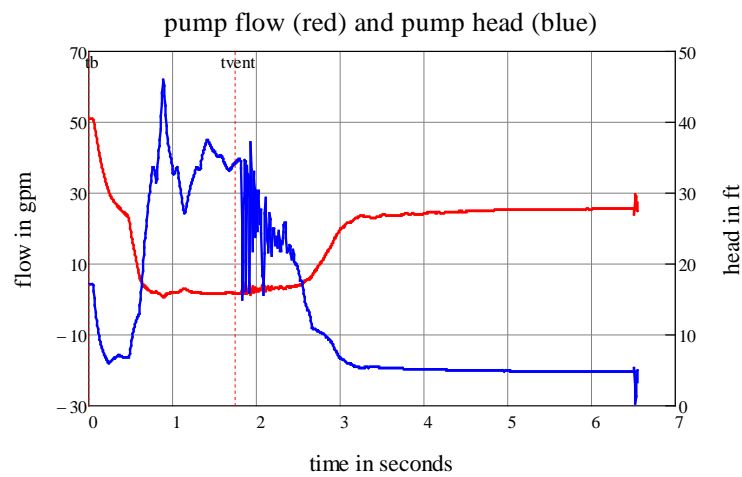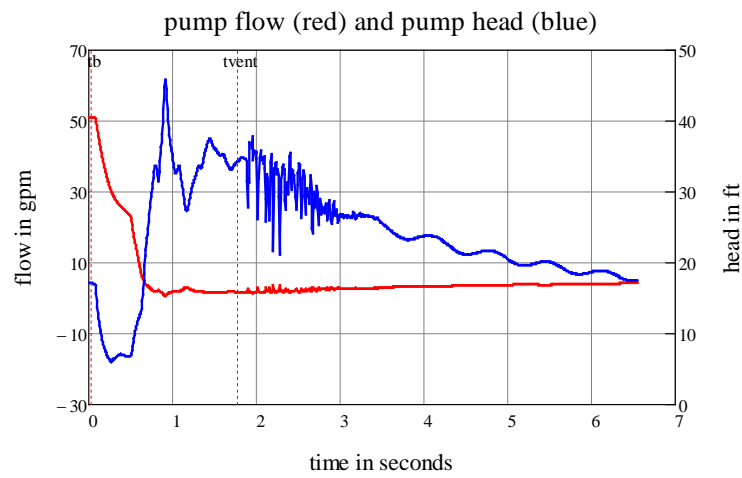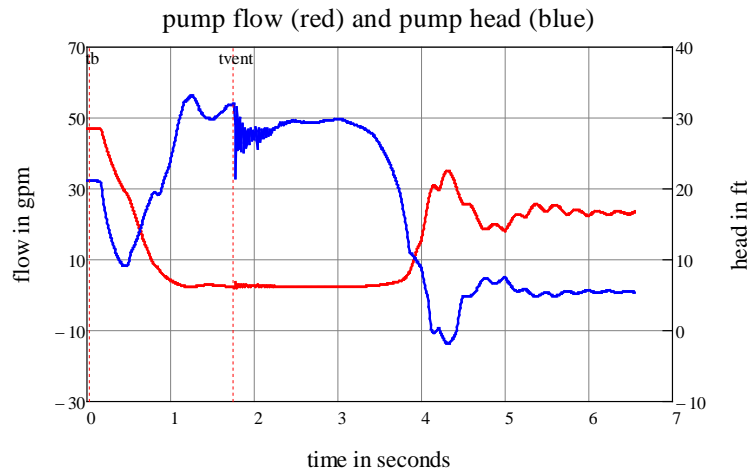
Figure 30 Comparison of flow and head through the pump for simulation cases 6-2 (top), 10-2 (middle), and 11-1 (bottom)
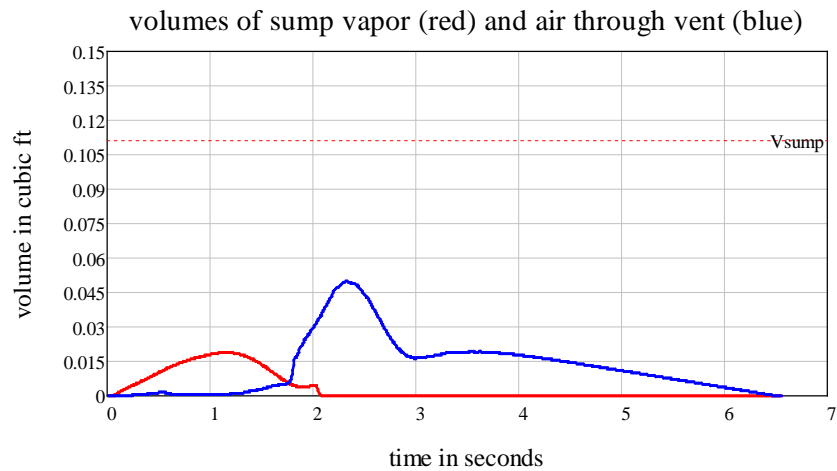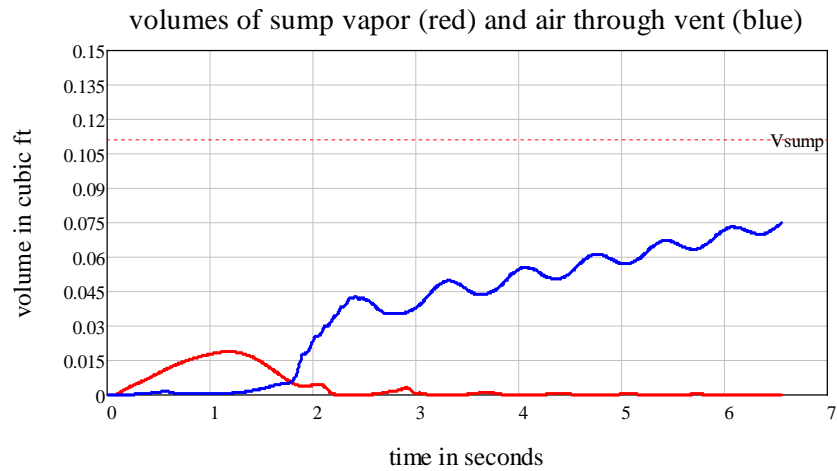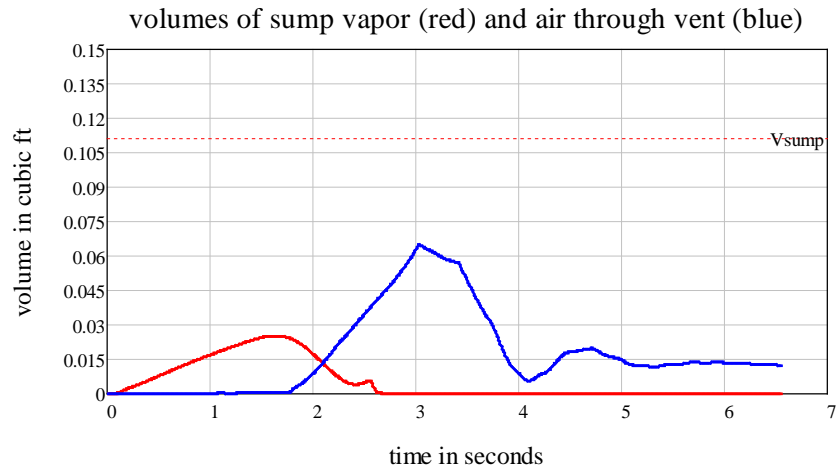
Figure 31 Comparison of cavity volume at the sump and at the air vent for simulation cases 6-2 (top), 10-2 (middle), and 11-1 (bottom)
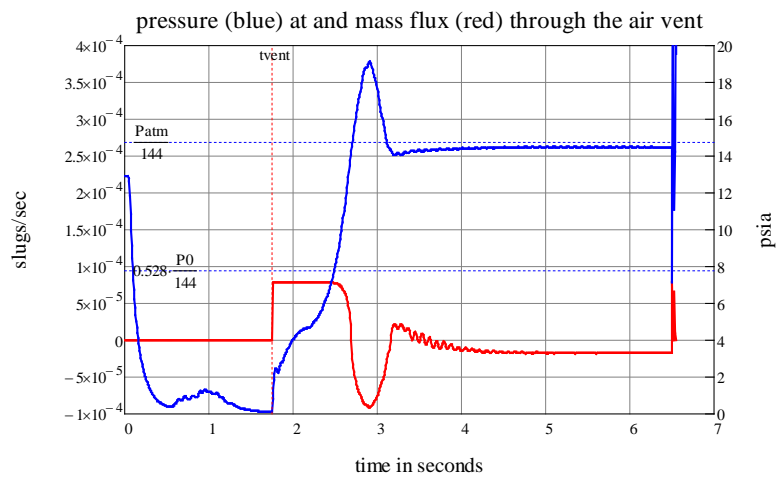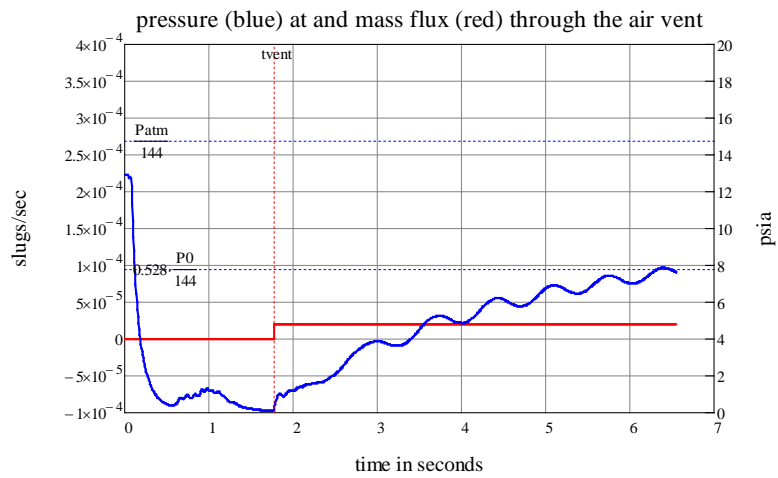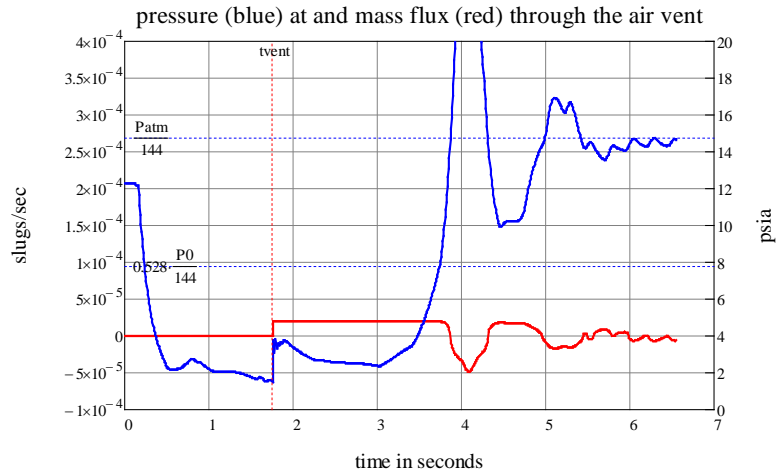
Figure 32 Comparison of air vent behavior between simulation cases 6-2 (top), 10-2 (middle), and 11-1 (bottom)

that corroborated with the above descriptions. We note that after the moment of air vent opening, *tvent*, a portion of the air mass flow trace is flat for all three cases. This is because, for the corresponding time period, the pressure in the pipe was so low that the sonic limit was exceeded, the air inflow to the pipe was choked, and the rate of air flow no longer depended on the pressure inside the pipe. In such a choked flow condition, the only way to increase the rate of air inflow is to increase the size of the air vent orifice. To see this, we compare the middle and bottom panels of Figure 32.   It is seen that the choked air inflow rate for Case 11-1 is four times the choked inflow rate for Case 10-2. This is consistent with the fact that the diameter of the orifice for Case 11-1 is twice the orifice diameter used in Case 10-2.   The plots also show periods of air being expelled from the pipe when the local pressure was above atmospheric.

14. Dual-Drain Simulations

A dual-drain system shown in Figure 1 was simulated. It was assumed that the two drains are identical so that the steady-state flow is equally divided between the two. The measured steady-state flow and pressures for Case 2 were used for dual-drain simulations. The IE foam was assumed to be lowered to the vicinity of the first drain and blocked the drain suddenly and completely at 0.735 seconds. The pump remained energized at all times. There is no dual-drain data to compare with. Only the simulated results are discussed below. The numerical model used for dual-drain simulations was previously submitted to CPSC in September 2009, as a part of the Interim Report.

Figure 33 shows the pressures at various locations and the pump rpm as before. It is seen that, with the second drain open, the first drain could not remain blocked with the parameters of Case 2. The disturbance to the pressures in the system is small and damped out quickly.

Figure 34 explains the dynamics of the blockage and the subsequent release of the IE foam. *Q1* represents the flow entering the connector between sump 1 and the "T" junction.   It is to be distinguished from the flow from pool into sump 1, which is zero once the drain is blocked. *P1* represents the gauge pressure at the first sump. The corresponding quantities for sump 2 are denoted as *Q2* and *P2*. *Q3* is the flow entering the suction pipe immediately downstream of the junction. *P3* is junction pressure. *S* represents the foam volume in sump 1 in cubic inches. In Figure 34, the flows are in gpm, and the pressures are in psig.

Blocking sump 1 causes different amounts of reduction in *P1*, *P2*, and *P3*, as shown. In the beginning, the flow from sump 1 is decelerated, while the flow from sump 2 is accelerated by these pressure differentials. *Q1* is reversed in this process. As *Q1* feeds sump 1, *P1* starts to recover, and the IE foam starts to retract.   The foam is released from sump 1 vacuum at about 0.866 seconds when *S* becomes zero (see the bottom panel of figure 34). After release, *P1* is at
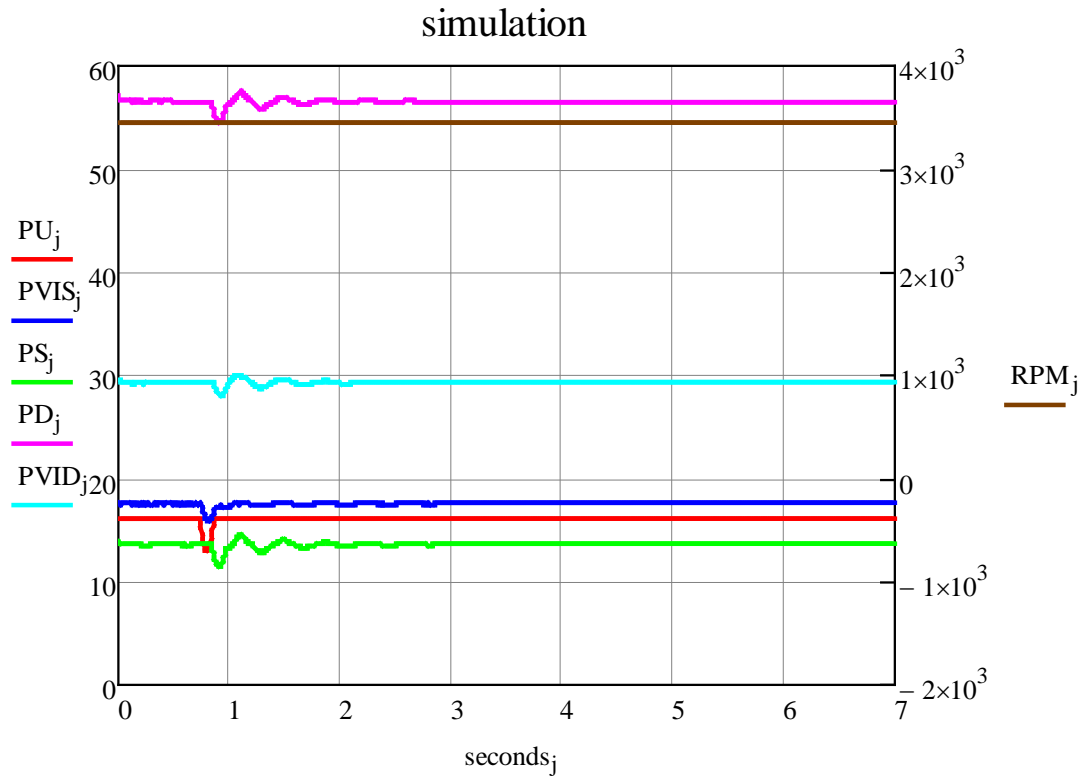
Figure 33 Disturbance produced by momentary blockage of one drain in a dual-drain system

pool pressure, which is higher than the junction pressure *P3*. As a result, the flow toward sump1 is being slowed down and then turned around. The original steady-state flow is soon reestablished after the momentary blockage.

The above simulation is an example of how dual drains could work to release vacuum. It is known to be possible for a blocker to be held down under certain conditions.

15. Conclusion

A numerical model for SVRS has been developed with the aids of physical test data and high-speed videos provided by CPSC. Favorable comparisons were obtained between model results and test data for both pump switch tests and for air vent tests.   This indicates that the model captures the main traits of SVRS and can be used to analyze SVRS under various conditions. The ability of the model to simulate dual-drain systems is demonstrated also. The model explains the complex dynamics involved and is helpful in understanding the dynamics of SVRS.
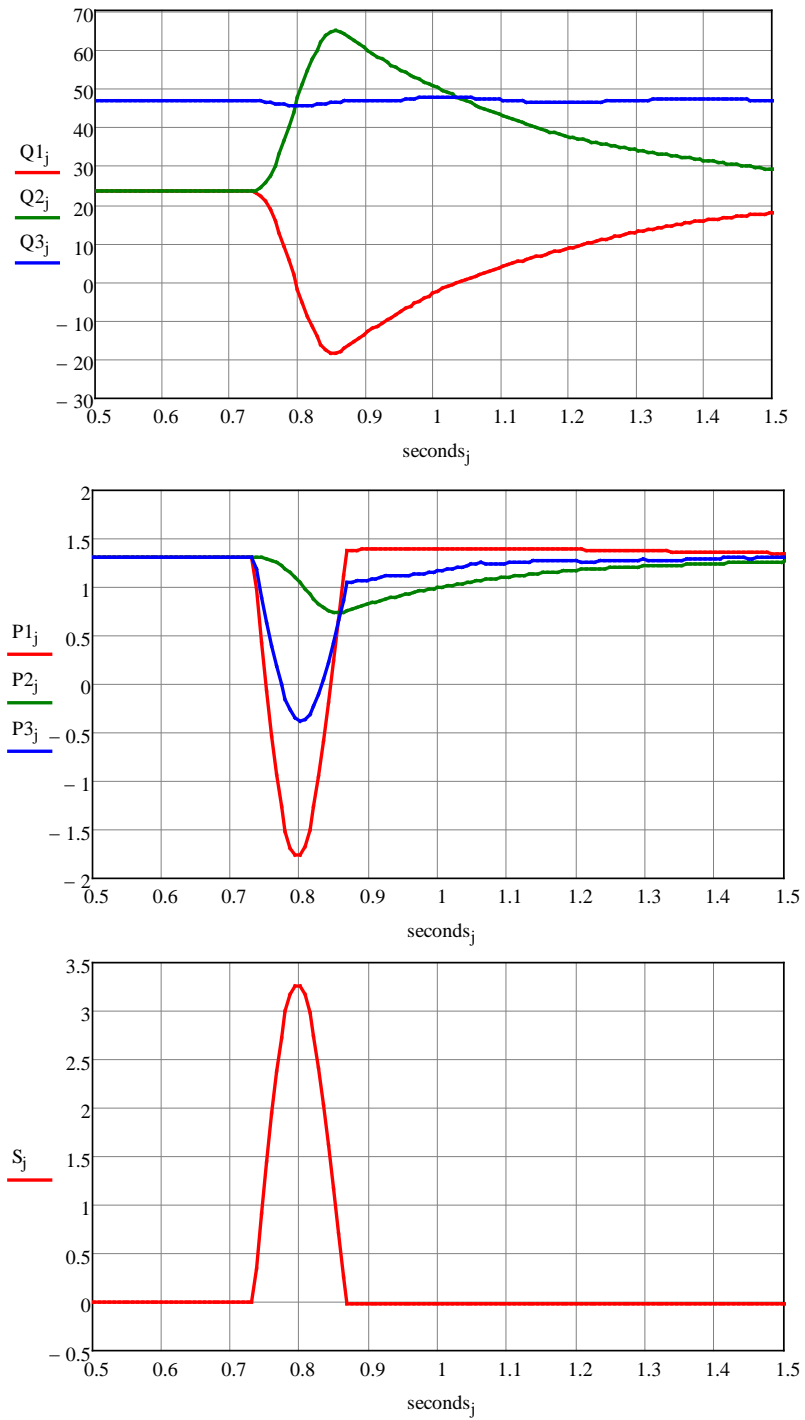
Figure 34 Details explaining the dynamics of dual-drain systems

16. The Numerical Model SVRS

The numerical model SVRS.xmcd and its data input module SVRS Data Input.xmcd are submitted in parallel with the submission of this report. These programs are written in Mathcad14 and must run with Mathcad14. The program input/output and its execution are explained in Appendix 2.

17. References

ASME, 2002, "Manufacture Safety Vacuum Release Systems (SVRS) for Residential and Commercial Swimming Pools, Spas, Hot tub, and Wading Pool Suction Systems - An American National Standard," ASME A112.19.17-2002.

ASTM, 2004, "Standard Specifications for Manufactured Safety Vacuum Release System (SVRS) for Swimming Pools, Spas, and Hot Tubs," ASTM Designation: F 2387-04.

RELAP5-3D Code Development Team, 2005, RELAP5-3D Code Manual Volume IV: Models and Correlations, INEEL-EXT-98-00834, pp. 3_309-3_317.

Road, E., Smith, W. L., and Black, J. A., 1982, Model Pump Performance Program – Data Report, NP-2379, Electric Power Research Institute, Palo Alto, CA.

Liou, Jim C. P., 2000, "Numerical Properties of the Discrete Gas Cavity Model for Transients," ASME Journal of Fluids Engineering, Vol. 122, September, pp. 636-639.

Liou, Jim C. P., 2009, "A Numerical Model for Safety Vacuum Release Systems (SVRS) – An Interim Report."

Wylie, E. B., 1984, "Simulation of Vaporous and Gaseous Cavitation," ASME Journal of Fluids Engineering, Vol. 106, September, pp 307-311.

Wylie, E. B., and Streeter, V. L., 1993, Fluid Transients in Systems, Prentice Hall, Englewood Cliffs, NJ.

18. Appendix 1 - Correspondence of case names with the original data file names

Case 1: P+F+O-S+T-M- no. 2 reduced.xls

Case 2: P+F-O-S-T+M-_no._4_reduced.xls

Case 3: P+F-O+S-T-M+_no.2_reduced.xls

Case 4: Phalf F+O-S-T-M+ no1 reduced.xls

Case 5: Phalf F+O-S-T-M+ no2 reduced.xls

Case 6_1: P_half_F+O-S+T+M+_B_0.14_No.1_Reduced.xls

Case 6_2: P half F+O-S+T+M+ B 0.14 No.2 Reduced.xls

Case 7: Air Vent Bore 0.14 P half F+O-S-T+M+ no.1 REDUCED.xls

Case 8: Air Vent Bore 0.21 P half F+O-S-T+M+ no.1 REDUCED.xls

Case 9_1: P half F+O-S-T+M+ B 0.21 No.1 Reduced.xls

Case 9_2: P_half_F+O-S-T+M+_B_0.21_No.2_Reduced.xls

Case 10_1: P half F+O-S-T+M+ B 0.14 No.1 Reduced.xls

Case 10_2: P half F+O-S-T+M+ B 0.14 No.2 Reduced.xls

Case 11_1: P half F+O-S-T+M+ B 0.28 No.1 Reduced.xls

Case 11_2: P_half_F+O-S-T+M+_B_0.28_No.2_Reduced.xls

19. Appendix 2 - SVRS Data Input, Execution, and Results Display

The program SVRS.xmcd and its data input module SVRS Data Input.xmcd need to be in the same directory. The input model uses text and list boxes to solicit data. It is a simple and short process. Once completed, the data are written into a text file with a .prn extension.

SVRS data Input.xmcd is shown on the next two pages. The input process starts by providing a case identification. The rest is self-explanatory. All the data needed to generate the simulated results can be found in Tables 1 and 2. After all the data have been entered, move the cursor to the bottom of the code to execute the module. The data will be written to a text file named after the case identification and with an extension .prn. This data file resides in the same directory.

To run SVRS.xmcd, enter the case identification into the text box at the beginning of the program, and move the cursor to the end of the program. A set of plots will be automatically generated by the program.

SVRS stores all the variables for results display, including head and flow data for animations. Running SVRS Data Input.xmcd and SVRS.xmcd requires Mathcad14. Some familiarity with Mathcad14 will be helpful in generating additional output, including head and flow animations.

SVRS Data Input Module (Jim Liou, June 28, 2010)

TEST CASE ID

case_name :=

Case 6_1

SYSTEM

Select suction pipe length (37 ft for short, 100 ft for long)

suction_pipe_length :=

short
long

Enter pump elevation offset

pump_elevation_offset_inches :=

-36

Enter tank depth

tank_depth_inches :=

34

Enter water temperature

water_temperature_degF :=

53

Select pump

pump_hp :=

1/2 hp Sta-Rite
3 hp Challenger

Select air vent size.

air_vent_size :=

not used
0.14 inch
0.21 inch
0.28 inch

Select "not used" if pump switch is used for vacuum release

STEADY-STATE FLOW

flow_rate_gpm :=

47

TIMING OF EVENTS

time_of_drain_blockage_sec :=

0.01

time_of_switching_pump_off_sec :=

9999

Enter a lage number if pump switch is not used

time_of_opening_air_vent_sec :=

1.776

Enter a large number if air vent is not used

VOID FRACTION OF UNDISOLVED AIR

void_fraction_of_free_air_in_pipes :=

| 0.0017 |

A reasonable value is 0.0017 or less

void_fraction_of_free_air_in_sump :=

| 0.0005 |

A reasonable value is 0.005 or less

DATA INPUT COMPLETED

PUTTING DATA INTO AN ARRAY

$$X := \begin{pmatrix} \text{suction\_pipe\_length} \\ \text{pump\_elevation\_offset\_inches} \\ \text{tank\_depth\_inches} \\ \text{water\_temperature\_degF} \\ \text{pump\_hp} \\ \text{air\_vent\_size} \\ \text{flow\_rate\_gpm} \\ \text{time\_of\_drain\_blockage\_sec} \\ \text{time\_of\_switching\_pump\_off\_sec} \\ \text{time\_of\_opening\_air\_vent\_sec} \\ \text{void\_fraction\_of\_free\_air\_in\_pipes} \\ \text{void\_fraction\_of\_free\_air\_in\_sump} \end{pmatrix}$$

WRITING THE DATA ARRAY INTO A FILE

concat(CWD, case_name) = "J:\air vent tests\Analysis\Case 6_1"

b := concat(CWD, case_name)

out := WRITEPRN(b, X)

out =

	0
0	100
1	-36
2	34
3	53
4	0.5
5	0.14
6	47
7	0.01
8	$9.999 \cdot 10^3$
9	1.776
10	$1.7 \cdot 10^{-3}$
11	$5 \cdot 10^{-4}$